Universidade Federal de Juiz de Fora

Engenharia Elétrica

Programa de Pós-Graduação em Engenharia Elétrica

Mateus de Lima Filomeno

Cooperative Communication for Broadband PLC and PLC/Wireless Systems: Achievable Data Rate Analyses

Juiz de Fora

2018

Ficha catalográfica elaborada através do Modelo Latex do CDC da UFJF com os dados fornecidos pelo(a) autor(a)

Filomeno, Mateus.

Cooperative Communication for Broadband PLC and PLC/Wireless Systems: Achievable Data Rate Analyses / Mateus de Lima Filomeno. – 2018.

62 f. : il.

Orientador: Moisés Vidal Ribeiro

Dissertação de Mestrado – Universidade Federal de Juiz de Fora, Engenharia Elétrica. Programa de Pós-Graduação em Engenharia Elétrica, 2018.

1. Comunicação via rede de energia elétrica. 2. Comunicação cooperativa. 3. Comunicação híbrida. 4. Comunicação sem fio. 5. Taxa de dados ergódica alcançável. I. Vidal Ribeiro, Moisés, orient. II. Título.

Mateus de Lima Filomeno

Cooperative Communication for Broadband PLC and PLC/Wireless Systems: Achievable Data Rate Analyses

Dissertação de mestrado apresentada ao Programa de Pós-Graduação em Engenharia Elétrica da Universidade Federal de Juiz de Fora, na área de concentração em sistemas eletrônicos, como requisito parcial para obtenção do título de Mestre em Engenharia Elétrica.

Orientador: Moisés Vidal Ribeiro

Juiz de Fora

2018

I dedicate this thesis to my family and friends. A special feeling of gratitude to my mother Roseny, my grandmother Neide, and my brother Lucas.

ACKNOWLEDGEMENTS

First and foremost, I would like to thank God for guiding me throughout my life and for being my greatest refuge in difficult times.

I would also like to thank to my mother Roseny de Lima Silva, my brother Lucas de Lima Filomeno, and my grandmother Neide de Araújo Lima, for always being by my side.

My special words of thanks go to my friend Lucas Giroto de Oliveira, for years of friendship and revision of this text, and to my friends of the LCOM who never hesitated in helping me and made me grow professionally and personally. Thank you all, guys.

Finally, my deepest thanks go to Professor Moisés Vidal Ribeiro, for his guidance throughout the development of this work, and to Professors Marcello Luiz Rodrigues de Campos and Fabrício Pablo Virgínio de Campos, for their valuable contributions.

"I press on toward the goal to win the prize for which God has called me heavenward in Christ Jesus."
(Philippians 3:14)

RESUMO

Esta dissertação tem como objetivo discutir as comunicações cooperativas híbrida e não híbrida aplicadas a sistemas de comunicação de dados em banda larga e em ambientes residenciais. Nesse sentido, o modelo de canal com retransmissor único em dois estágios é investigado para sistemas de comunicação em banda larga através da rede de energia elétrica. Este modelo de canal cooperativo é formado pela concatenação de dois canais com retransmissor único, cobrindo enlaces de comunicação de dados com até dois saltos. Além disso, um modelo de canal híbrido com retransmissor único, utilizando rede elétrica e ar, é analisado para sistemas de comunicação de dados em banda larga em que enlaces de até um salto são considerados. Expressões de taxas de dados alcançáveis ergódicas são derivadas para os modelos de canais cooperativos híbridos e não híbridos, a fim de compará-los. Devido às características de canais e ruído das redes de energia elétrica, os resultados numéricos são baseados em um conjunto de dados constituído por estimativas de canais e medições de ruído cobrindo a faixa de frequência de $1,7$ a 100 MHz e diferentes posições do nó retransmissor. Para os canais sem fio, o modelo HIPERLAN/2 com a mesma largura de banda é utilizado, considerando uma freqüência central de 5 GHz, enquanto o ruído aditivo é considerado branco gaussiano. Com relação aos sistemas de comunicação através da rede energia elétrica, mostra-se que o modelo de canal com retransmissor único em dois estágios é a melhor opção quando o enlace da fonte ao destino encontra-se severamente degradado (por exemplo, alta atenuação de sinal devido à longa distância entre nós fonte e destino e/ou presença de ruído de alta potência). Quando a degradação do canal não é acentuada, o modelo de canal de dois saltos é mais apropriado. Acerca dos sistemas híbridos, constata-se que, quando o retransmissor está no meio do caminho entre fonte e destino, o modelo de canal híbrido com retransmissor único apresenta o melhor desempenho em termos de taxa de dados alcançável ergódica, enquanto o modelo de canal híbrido de um salto oferece os melhores resultados para outros casos.

Palavras-chave: Comunicação cooperativa. Comunicação híbrida. Comunicação via rede elétrica. Comunicação sem fio. Taxa de dados ergódica alcançável.

ABSTRACT

This dissertation aims to discuss hybrid and non-hybrid cooperative communications applied to in-home broadband data communication systems. In this sense, the two-stage single-relay channel model is investigated for in-home broadband power line communication systems. This cooperative channel model consists of the concatenation of two single-relay channels, covering data communication links with up to two hops. Moreover, a hybrid power line/wireless single-relay channel model is analyzed for broadband data communication systems, considering one-hop links. Ergodic achievable data rate expressions are derived for both hybrid and non-hybrid cooperative channel models in order to compare them. Due to channel and noise characteristics of electric power grids, numerical results are based on a data set constituted by power line channel estimates and additive noise measurements covering the frequency band from 1.7 up to 100 MHz and different relay positions. For wireless channels, the HIPERLAN/2 model with the same bandwidth is used, but at a central frequency of 5 GHz, while the additive noise is considered to be Gaussian white. Regarding only power line communication systems, it is shown that the two-stage single-relay channel model is the best option when the source-to-destination link is severely degraded (e.g., high signal attenuation due to the long distance between source and destination nodes and/or high-power noise presence). When the channel degradation is not severe, the two-hop channel model is more appropriate. Concerning hybrid systems, it is observed that, when the relay is halfway between source and destination nodes, the hybrid single-relay channel model presents the best performance in terms of ergodic achievable data rate, while the hybrid one-hop channel model yields the best results for other cases.

Key-words: cooperative communication, hybrid communication, power line communication, wireless communication, ergodic achievable data rate.

LIST OF FIGURES

Figure 1 – Two-stage single-relay channel model during one symbol time duration. 17
Figure 2 – Adopted configurations from the 2S-SRC model. 18
Figure 3 – Adopted hybrid channel models. 25
Figure 4 – PSD of an additive noise measurement in $\mathcal{SD}$, $\mathcal{SR}$, and $\mathcal{RD}$ channels. . 33
Figure 5 – $\beta_1 \times \beta_2$ plane used to organize the data set in the four cases 34
Figure 6 – AF protocol and $G_{SD} = -80$ dB: Ergodic achievable data rate gain vs total transmission power. 37
Figure 7 – DF protocol and $G_{SD} = -80$ dB: Ergodic achievable data rate gain vs total transmission power. 39
Figure 8 – AF protocol and $\rho_B/\rho_E \times G_{SD}$. 41
Figure 9 – DF protocol and $\rho_B/\rho_E \times G_{SD}$. 42
Figure 10 – Without combination: Ergodic achievable data rate gain vs total transmission power. 45
Figure 11 – With combination: Ergodic achievable data rate gain vs total transmission power. 46
Figure 12 – Magnitude of average PLC CFRs. 60
Figure 13 – Magnitude of average wireless CFRs 61

LIST OF TABLES

Table 1 – Decision matrices for MRC in the first and second time slots. 55
Table 2 – Decision matrices for MRC in the third and fourth time slots. 58
Table 3 – Specification of the 18-path HIPERLAN/2 for typical office environments. 59

ACRONYMS

2S-SRC two-stage single-relay channel

AWGN additive white Gaussian noise

AF amplify-and-forward

CFR channel frequency response

CIR channel impulse responses

CSI channel state information

DF decode-and-forward

DFT discrete Fourier transform

HIPERLAN high-performance radio local area network

HS-OFDM hermitian-symmetric orthogonal frequency-division multiplexing

HSRC hybrid single-relay channel

HOHC hybrid one-hop channel

LGRC linear Gaussian relay channel

LTI linear time-invariant

MIMO multiple-input multiple-output

MRC maximum ratio combining

N**-CGRC** N-block circular Gaussian relay channel

PLC power line communication

PSD power spectral density

SNR signal-to-noise ratio

SRC single-relay channel

TDMA time-division multiple access

CONTENTS

1	**INTRODUCTION**	**12**
1.1	OBJECTIVES	14
1.2	THESIS ORGANIZATION	15
1.3	SUMMARY	15
2	**TWO-STAGE SINGLE-RELAY CHANNEL MODEL**	**16**
2.1	PROBLEM FORMULATION	16
2.2	ERGODIC ACHIEVABLE DATA RATE	19
2.2.1	**Configuration** A	19
2.2.2	**Configuration** B	20
2.2.3	**Configurations** C **and** D	21
2.2.4	**Configuration** E	22
2.3	SUMMARY	22
3	**HYBRID PLC/WIRELESS CHANNEL MODELS**	**24**
3.1	PROBLEM FORMULATION	25
3.2	ERGODIC ACHIEVABLE DATA RATE	26
3.2.1	**Hybrid One-Hop Channel Model**	27
3.2.2	**Hybrid Single-Relay Channel Model**	29
3.3	SUMMARY	31
4	**NUMERICAL RESULTS**	**33**
4.1	TWO-STAGE SINGLE-RELAY CHANNEL MODEL	35
4.1.1	**Ergodic Achievable Data Rate vs Total Transmission Power**	36
4.1.2	**Ergodic Achievable Data Rate vs Average Channel Gain of the Direct Link**	38
4.2	HYBRID PLC/WIRELESS COOPERATIVE CHANNEL MODELS	43
4.2.1	**Ergodic Achievable Data Rate Without Combination**	43
4.2.2	**Ergodic Achievable Data Rate With Combination**	44
4.3	SUMMARY	47
5	**CONCLUSIONS**	**48**
5.1	Future works	49
	REFERENCES	**50**

APPENDIX A – AF and DF achievable data rates 55

APPENDIX B – SNR for configuration E 57

APPENDIX C – Specification of the 18-path HIPERLAN/2 for typical office environments. 59

APPENDIX D – PLC Channel Frequency Responses 60

APPENDIX E – Wireless Channel Frequency Responses . . . 61

APPENDIX F – List of Publications 62

1 INTRODUCTION

Currently, a challenging and timely research question is how to support the increasing demands of society and machines for connectivity that can fulfill previous and new kind of applications, such as broadband and narrowband communications with different trade-off among data rate, packet size, real or non-real time, energy availability, and spectrum scarcity. This research question leads to the emergence of novel energy-efficient, low-cost, flexible, and powerful data communication technologies and the improvement of existing ones. Among several technologies under investigation and improvement, power line communication (PLC) [1–7] and wireless communication [8–10] have received considerable attention due to their low-cost and suitability for fulfilling the needs and demands of Internet of Things, Smart Grids, and Smart Cities. While the former technology takes advantage of the ubiquitous presence of electric power grids [11, 12], the latter does not require infrastructures for connecting devices.

Nonetheless, some challenges related to both technologies need to be pursued for maximizing their usage as data communication media. Regarding electric power grids, the main challenges are impedance mismatching, frequency selectivity of PLC channels, increasing signal attenuation along with both frequency and distance, high-power impulsive noise presence, dynamics of loads, electromagnetically unshielded power lines, and regulatory constraints [13–15]. Concerning wireless communication, besides high dependence on line-of-sight propagation and vulnerability to non-authorized access, it is worth mentioning the increasing signal attenuation along with both distance and carrier frequency, the susceptibility to interference among two or more systems operating in the same frequency band, the scarcity of spectrum, and the lack of reliable atmospheric conditions.

In this context, cooperative communication [16, 17], which was initially developed to allow single-antenna devices to benefit from multiple-input multiple-output (MIMO) system features [10], has been widely investigated as one of the alternatives to counterbalance the disadvantages of data communication performed over electric power grids [18–21] and air [22–24]. In this regard, amplify-and-forward (AF) and decode-and-forward (DF) protocols have been the most reported in the literature [25–29]. Moreover, hybrid PLC/wireless systems have also been investigated as an alternative to improve data communication performance [30–32] since it can take advantage of both electric power grids and air to improve data rate and reliability between source and destination nodes under several circumstances, see [33]. In such data communication systems, electric power grids and wireless media are used simultaneously in a complementary way in order to maximize the available channel resources and fulfill data communication constraints.

Regarding cooperative communication, an important issue is related to the cooperative channel model. Many models have been addressed in the literature, the most

common being those with a single relay between edge nodes (the ones that are not relays). The simplest of them is called two-hop channel model, in which the relay is located between source and destination nodes and the direct link can be either existing [34] or non-existing [35]. Based on this model, [36] addressed a two-way channel model that is used in two phases: in the first one, the edge nodes perform data transmission towards the relay node, while in the second one, the relay node sends data towards the edges. Even more popular than the aforementioned models, the single-relay channel (SRC) model [20,28] considers that the relay is not exactly in between source and destination nodes, but rather connected by a branch point. With respect to the cooperative channel models with more than one relay, the multihop is the most investigated [18, 26]. It consists of multiple nodes between transmitter and receiver and considers that the direct link does not exist, i.e., each relay receives the signal only from its predecessor and forwards it to the subsequent relay until the signal reaches the destination node. Also, [37] addressed a cooperative channel model with several relays between source and destination nodes, proposing a method to find the best one to be used.

On the subject of hybrid PLC/wireless systems, there are several works addressing this topic in the literature [30, 31, 33, 38–46]. Among them, different types of hybrid communication are shown. For instance, [38–40] focused on PLC and wireless technologies working in cascade so that the end-to-end data rate is bounded by the smallest one considering both channels. In such works, a node between source and destination is required, since there must be a device able to receive data at the output of the first channel and transmit through the other. More recently, [41] introduced a new concept of hybridism in which PLC and wireless channels are used in cascade without a intermediate node. Basically, transceivers are connected to electric power grids and to the air. They communicate with each other because both of them occupy the same frequency band starting in 1.7 MHz and ending in 100 MHz. According to [41], as the signal transmitted by a PLC device is irradiated from unshielded power lines, a wireless receiver and a PLC transmitter can be connected wirelessly. Another kind of hybridism associated with PLC and wireless communication refer to the use of these channels in parallel [33,43–46], which proved to be able to improve data communication performance in terms of data rate [43,46] and reliability [33,44,45].

Although some works have already pointed out the benefits of cooperative communication for PLC systems, a cooperative channel model resulting from the concatenation of two SRC models has not been discussed yet. Shortly, this channel model is characterized by using the destination node of a first SRC model as the source node of a second SRC model, resulting in a cooperative channel model with five nodes: source, destination, and three relays; which is named two-stage single-relay channel (2S-SRC) model. Using the same argument, the nS-SRC model ($n > 2$) can be easily defined; however, this work will drive attention over the 2S-SRC model because the use of up to two-hop data com-

munication links makes sense when in-home broadband PLC systems are considered. As a matter of fact, data communication links with up to two hops within a home means that the distance between the edge nodes (source and destination nodes) is twice the one addressed in [20] and, as a consequence, the signal degradation between these nodes is much more severe. It means that it is worth investigating this scenario since up to two-hop links are feasible for performing in-home broadband data communication (i.e., frequency band is from 1.7 up to 100 MHz) due to the distances involved.

Furthermore, [30,31,33] analyzed the narrowband hybrid PLC/wireless SRC model (i.e., a SRC model in which all nodes can perform data communication through both PLC and wireless channels) for dealing with low-bit-rate applications. In that case, a narrow frequency bandwidth of 500 kHz was considered. The frequency band used by PLC and wireless communication was between 0 and 500 kHz and between 915 MHz and 915.5 MHz, respectively. The adopted channel models showed that, for these frequency bands, PLC channels are frequency-selective, while the wireless channels are almost flat. Given some assumptions to ensure that only the channel diversity would be evaluated, it was shown that this kind of model can significantly improve the performance of a data communication system. Nonetheless, it is needed to verify whether this result is valid for a broadband hybrid PLC/wireless data communication system in which the frequency bandwidth is around 100 MHz. The broadband PLC is a baseband system that extends from 1.7 up to 100 MHz, while the broadband wireless communication is a passband system with carrier frequency at 5 GHz. As a consequence, both PLC and wireless channels are frequency-selective, which is different from the narrowband hybrid PLC/wireless investigations discussed in [30, 31].

1.1 OBJECTIVES

Given the aforementioned discussion and motivations related to cooperative and hybrid PLC/wireless data communication, the main objectives of this thesis are summarized as follows:

- To investigate the usefulness of the 2S-SRC model for in-home broadband PLC systems by analyzing performances in terms of ergodic achievable data rate and considering different values of total transmission power, average channel gain of the direct link, and relative relays positions. Based on a data set from a measurement campaign, which is constituted by thousands of PLC channel estimates and several additive noise measurements, to provide concrete and realistic analyses that are suitable for PLC designers and practitioners involved with broadband data communication.

- To analyze hybrid PLC/wireless channel models for broadband data communication

within a home, deriving closed-form expressions for their ergodic achievable data rates and evaluating their performances for different values of total transmission power with the use of a measured data set of channels and additive noise for the PLC branch, and the high-performance radio local area network (HIPERLAN)/2 channel model [47] corrupted by additive white Gaussian noise (AWGN) for the wireless branch.

1.2 THESIS ORGANIZATION

The remainder of this document is organized as follows:

- Chapter 2 describes the 2S-SRC model for in-home broadband PLC systems. The most discussed cooperative channel models of the literature for PLC systems [28, 29, 34, 35], which are obtained from the 2S-SRC model, are also addressed. Closed-form expressions for their ergodic achievable data rates are derived by considering AF and DF cooperative protocols.
- Chapter 3 outlines hybrid channel models based on PLC and wireless communication systems. A formulation for the hybrid SRC model and the hybrid one-hop channel model is presented. Closed-form expressions for their ergodic achievable data rates are derived by considering the lack of signal combining as well as its presence. AF protocol is employed in this chapter.
- Chapter 4 shows numerical analyses regarding the in-home broadband data communication systems described in Chapters 2 and 3. Considering different values of total transmission power, average channel gain of the direct link, and relative relays positions, comparative numerical analyses are carried out in terms of ergodic achievable data rate.
- Chapter 5 places concluding remarks of this thesis. Also, it outlines future works.

1.3 SUMMARY

This chapter has presented a brief introduction of this thesis, addressing important aspects of cooperative and hybrid communication applied to both PLC and wireless communication systems. Also, the main objectives and the organization of this work have been summarized.

2 TWO-STAGE SINGLE-RELAY CHANNEL MODEL

Several works have discussed the gains associated with the use of cooperative communication for improving the performance of in-home narrowband and broadband PLC systems [18, 20, 28]. The majority of them adopt well-known channel models in which PLC channels are random process [26, 28, 35]. A worthy remark regarding these PLC channel models is the fact that they consider frequency-domain representations in which the PLC channel is either flat or an stationary random process. Nevertheless, surveys on electric power grid measurements have shown that an extensive investigation has to be worldwide carried out to come up with representative PLC channel models. Trying to exploit this issue, [20] analyzed the cooperative communication adopting a data set constituted by several PLC channel estimates and additive noise measurements, which were obtained from a measurement campaign carried out in several Brazilian residences. Based on this data set, [20] discussed the suitability of the SRC model for in-home broadband data communication by addressing distances between source and destination nodes that cover up to one-hop links; however, the data set has shown that data communication covering up two-hop links has to be addressed since they cover distances in which the signal attenuation through in-home electric circuits is relevant.

In this regard, this chapter investigates the 2S-SRC model and compares its ergodic achievable data rate against the ones from others cooperative channel models discussed in the literature for in-home broadband PLC systems. A formulation of the 2S-SRC model regarding in-home PLC system covering the frequency band from 1.7 up to 100 MHz is presented. Similar to [20], [48, 49] are used to derive the ergodic achievable data rates of five configurations of the 2S-SRC model as it allows to precisely take into account the frequency selectivity of PLC channels and the nonwhiteness of the additive noise in electric power grids.

This chapter is organized as follows: Section 2.1 outlines the problem formulation, describing the cooperative channel models adopted in this chapter. In the sequel, Section 2.2 derives their ergodic achievable data rates, assuming AF or DF protocol at the relay node, as well as maximum ratio combining (MRC) technique to combine the signals at the destination node. Section 2.3 addresses a brief summary on this chapter.

2.1 PROBLEM FORMULATION

The 2S-SRC model, shown in Fig. 1, is constituted by five nodes: one source node (S); three relay nodes (R_a, R_b, and R_c); and one destination node (D). From this model, active (perform data transmission) and inactive (receive data) relays between source and destination nodes define eight distinct configurations. However, discussing all possible configurations would be rather confusing, as a large number of configurations and

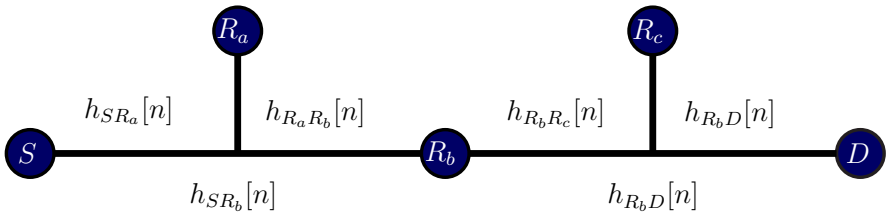

Figure 1: Two-stage single-relay channel model during one symbol time duration.

active relays are possible. Then, this chapter focuses on the 2S-SRC model, considering configurations with at most one active relay besides the 2S-SRC itself, as they are the most studied in the literature. Therefore, the investigated configurations, which are shown in Fig. 2, are described as follows:

- Configuration A: it is the one-hop channel model or the direct link. In this configuration all relays are inactive.
- Configuration B: it is the two-hop channel model [35]. It assumes that R_b node is active, while R_a and R_c nodes are inactive.
- Configuration C: it is the SRC model [20]. Basically, R_a node is active, while R_b and R_c nodes are inactive.
- Configuration D: it is the SRC model [20]. Essentially, R_c node is active, while R_a and R_b nodes are inactive.
- Configuration E: it is the 2S-SRC model, in which all relays are active.

To mathematically formulate the 2S-SRC model and its configurations, $T_C \gg T_S$, where T_C denotes the coherence time of the PLC channel and T_S is the symbol time interval. Moreover, the time-division multiple access (TDMA) method is used to access the channel since it is simple and very common in the literature [50, 51]. Then, each transmitter node (source and active relays) has one time slot from a total of N_T time slots, with $N_T \in \mathbb{N}^*$ being defined as the number of transmitters in the analyzed configuration, to send information. Also, S and R_b nodes take advantage of the broadcasting characteristic of electric power grids; however, due to the high attenuation of some channels, R_c and D nodes disregard all information received before R_b node performs its data transmission in the case R_b node is active (configurations B and E). For instance, in configuration E, S node broadcasts the original information to R_a and R_b nodes during the first time slot. In the following time slot, R_a node forwards the information to R_b node. In the third time slot, R_b node broadcasts the information to R_c and D nodes. At last, in the fourth time slot, R_c node sends the information to D node.

Now, let the PLC channels be linear time-invariant (LTI) within a symbol time duration and the channel impulse responses (CIR) be represented by $\{h_{ij}[n]\}_{n=1}^{L_{ij}}$, in which

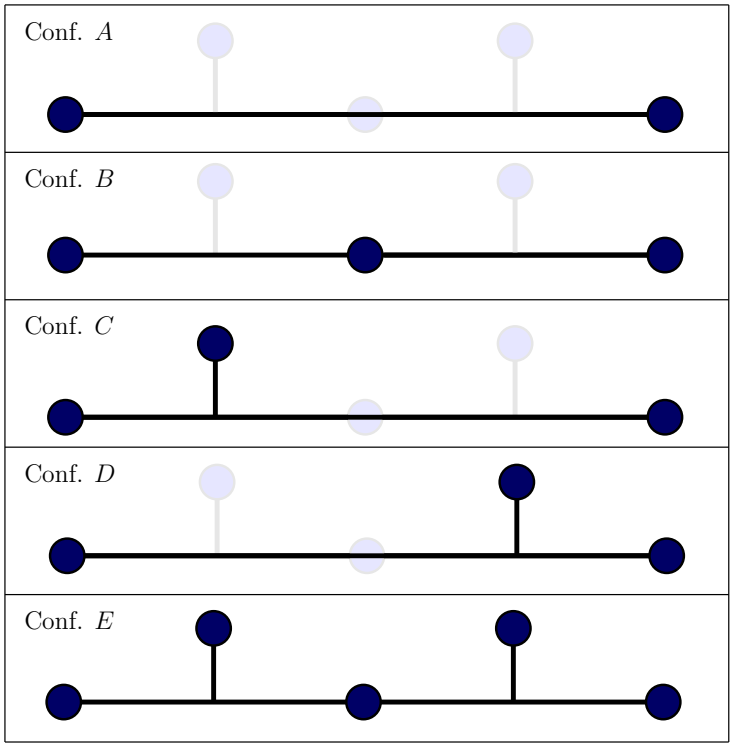

Figure 2: Adopted configurations from the 2S-SRC model.

L_{ij} is the length of the channel $\{h_{ij}[n]\}$, $i \in \{S, R_a, R_b, R_c\}$ denotes the transmitter node and $j \in \{R_a, R_b, R_c, D\}$ denotes the receiver node. To be algebraically manipulated, the CIRs are represented as $\mathbf{h}_{ij} = [h_{ij}[1]\ h_{ij}[2]\ ...\ h_{ij}[L_{ij}]]^T$. Also, the N-length vector that represents the channel frequency response (CFR) associated with $\mathbf{h}_{ij}$ is expressed as

$$\mathbf{H}_{ij} = \mathbf{W}_N \begin{bmatrix} \mathbf{I}_{L_{ij}} \\ \mathbf{0}_{(N-L_{ij})\times N} \end{bmatrix} \mathbf{h}_{ij}, \tag{2.1}$$

where $\mathbf{W}_N \in \mathbb{C}^{N\times N}$ denotes the N-size discrete Fourier transform (DFT) matrix, $\mathbf{I}_L \in \mathbb{R}^{L\times L}$ denotes an L-size identity matrix and $\mathbf{0}_{L\times Q}$ is a $L \times Q$ null matrix. Additionally, define the diagonal matrices $\mathbf{\Lambda}_{\mathbf{H}_{ij}} \triangleq \mathbf{diag}\{H_{ij}[1], H_{ij}[1], ..., H_{ij}[N]\}$ and $\mathbf{\Lambda}_{|\mathbf{H}_{ij}|^2} \triangleq \mathbf{\Lambda}_{\mathbf{H}_{ij}}\mathbf{\Lambda}^{\dagger}_{\mathbf{H}_{ij}}$, in which $H_{ij}[k]$ is the k-th element of $\mathbf{H}_{ij}$, $\forall\ k \in \{1, 2, ..., N\}$, and $\dagger$ denotes the conjugate transpose operator.

Let $\mathbf{X} \in \mathbb{C}^{N\times 1}$ and $\mathbf{V}_{ij} \in \mathbb{C}^{N\times 1}$ be random vectors that represent, in the frequency domain, the symbol transmitted by S node and the additive noise at the output of the channel associated with i and j nodes. Next, given that $\mathbb{E}\{\cdot\}$ denotes the expectation operator, it is assumed that $\mathbb{E}\{\mathbf{X}\} = \mathbf{0}_{1\times N}$, $\mathbf{R}_{\mathbf{XX}} = \mathbb{E}\{\mathbf{X}\mathbf{X}^{\dagger}\} = N\mathbf{I}_N$, in which $\mathbf{R}_{\mathbf{MM}}$ represents the autocorrelation matrix of a finite-length random vector $\mathbf{M}$. Also, $\mathbb{E}\{\mathbf{V}_{ij}\} = \mathbf{0}$, and $\mathbb{E}\{\mathbf{V}_{ij} \odot \mathbf{V}_{pq}\} = \mathbb{E}\{\mathbf{V}_{ij}\} \odot \mathbb{E}\{\mathbf{V}_{pq}\}$, $\forall ij \neq pq$, where $\odot$ denotes the Hadamard product. It is also considered that $\mathbb{E}\{\mathbf{V}_{ij}\mathbf{V}^{\dagger}_{ij}\} = N\mathbf{\Lambda}_{P_{\mathbf{V}_{ij}}}$, in which $\mathbf{\Lambda}_{P_{\mathbf{V}_{ij}}} \triangleq \mathbf{diag}\{P_{\mathbf{V}_{ij}}[1], P_{\mathbf{V}_{ij}}[2], ..., P_{\mathbf{V}_{ij}}[N]\}$ and $P_{\mathbf{V}_{ij}}[k]$ denotes the power of the k-th element of $\mathbf{V}_{ij}$, $\forall\ k \in \{1, 2, ..., N\}$. Following, let $P_S \geq 0$, $P_{R_a} \geq 0$, $P_{R_b} \geq 0$, and $P_{R_c} \geq 0$

be the transmission powers allocated to S, R_a, R_b, and R_c nodes, respectively. The sum power constraint criterion is satisfied as follows:

$$\sum_i P_i \leq P, \tag{2.2}$$

in which $P \geq 0$ is the total transmission power. Next, $\mathbf{\Lambda}_{\sqrt{P_i}} \triangleq \mathbf{diag}\{\sqrt{P_i[1]}, \sqrt{P_i[2]}, ..., \sqrt{P_i[N]}\}$ and $\mathbf{\Lambda}_{P_i} \triangleq \mathbf{diag}\{P_i[1], P_i[2], ..., P_i[N]\}$, where $P_i[k] \geq 0$ is the power allocated to the k-th subchannel at i-th node, $\forall\ k \in \{1, 2, ..., N\}$.

Given the sum power constraint criterion and the TDMA method, the following research questions emerge: "What kind of improvement can the 2S-SRC model offer when the distance between edge nodes within a home corresponds to data communication links with up to two hops?", "What kind of configuration can achieve the highest ergodic achievable data rate?" For answering these questions, Section 2.2 derives ergodic achievable data rate expressions for each configuration based on the aforementioned formulation.

2.2 ERGODIC ACHIEVABLE DATA RATE

This section outlines expressions for the ergodic achievable data rate of the five aforementioned configurations using AF or DF at the relay node together with MRC at the destination node. To do so, every configuration is modeled as a linear Gaussian relay channel (LGRC) [48] with finite memory $L_{\max} \in \mathbb{N} | L_{\max} \geq \max_{i,j}\{L_{ij}\}$. However, in PLC environment, noise is colored and CIRs have memory, which results in inter-block interference and, as a consequence, the evaluation of the achievable data rate for a LGRC model is very difficult. To overcome this problem, a recourse to N-block circular Gaussian relay channel (N-CGRC) [49], which eliminates the inter-block interference for $N \geq L_{\max}$, is recommended. Note that the achievable data rate associated with LGRC tends to be equal to that for N-CGRC as $N \to \infty$. Moreover, perfect symbol synchronization at the receiver side and complete channel state information (CSI) at both transmitter and receiver sides applies. The adoption of complete CSI allows the use of water-filling technique for maximizing the data rate associated with each channel model.

2.2.1 **Configuration** A

Let

$$\mathbf{Y}_D = \mathbf{\Lambda}_{\sqrt{P_S}} \mathbf{\Lambda}_{\mathbf{H}_{SD}} \mathbf{X} + \mathbf{V}_{SD} \tag{2.3}$$

be a complex random vector that models the received symbol at D node in the frequency domain. Also, $\mathbf{X}$ and $\mathbf{V}_{SD}$ are Gaussian random vectors. According to [52], the mutual information between transmitted and received symbols is expressed as

$$\begin{aligned} I(\mathbf{X};\mathbf{Y}_D) &= h(\mathbf{Y}_D) - h(\mathbf{Y}_D|\mathbf{X}) \\ &= h(\mathbf{Y}_D) - h(\mathbf{\Lambda}_{\sqrt{P_S}}\mathbf{\Lambda}_{\mathbf{H}_{SD}}\mathbf{X}|\mathbf{X}) - h(\mathbf{V}_{SD}|\mathbf{X}) \\ &= h(\mathbf{Y}_D) - h(\mathbf{V}_{SD}), \end{aligned} \tag{2.4}$$

where $h(\cdot)$ denotes the entropy operator over a random vector and $h(\mathbf{\Lambda}_{\sqrt{P_S}}\mathbf{\Lambda}_{\mathbf{H}_{SD}}\mathbf{X}|\mathbf{X}) = 0$. In addition, the entropy of $\mathbf{Y}_D$ and $\mathbf{V}_{SD}$ are, respectively, given by

$$h(\mathbf{Y}_D) = \log_2[(\pi e)^N \det(\mathbf{R}_{\mathbf{Y}_D\mathbf{Y}_D})] \tag{2.5}$$

and

$$h(\mathbf{V}_{SD}) = \log_2[(\pi e)^N \det(\mathbf{R}_{\mathbf{V}_{SD}\mathbf{V}_{SD}})]. \tag{2.6}$$

Therefore, the mutual information is expressed as

$$I(\mathbf{X};\mathbf{Y}_D) = \log_2[\det(\mathbf{I}_N + \mathbf{\Lambda}_{\gamma_{SD}})], \tag{2.7}$$

in which $\mathbf{\Lambda}_{\gamma_{ij}} = \mathbf{\Lambda}_{P_i}\mathbf{\Lambda}_{|\mathbf{H}_{ij}|^2}/\mathbf{\Lambda}_{P_{\mathbf{V}_{ij}}}$ is the signal-to-noise ratio (SNR) matrix associated with the channel between i and j nodes.

As the mutual information is maximized when $\mathbf{X}$ is a Gaussian random vector, the ergodic achievable data rate for configuration A is given by

$$C_A = \mathbb{E}_{\mathbf{H}}\left\{\max_{\mathbf{\Lambda}_{P_i}} \frac{B_w}{N\,N_T}\log_2[\det(\mathbf{I}_N + \mathbf{\Lambda}_{\gamma_{SD}})]\right\}, \tag{2.8}$$

subject to $\sum_i \mathrm{Tr}(\mathbf{\Lambda}_{P_i}) \leq P$, with $i \in \{S\}$ and $N_T = 1$. Note that $\mathbb{E}_{\mathbf{H}}\{\cdot\}$ denotes the expectation operator in relation to the CIRs that constitute the current configuration, $\mathrm{Tr}(\cdot)$ denotes the trace operator, and B_w is the frequency bandwidth.

2.2.2 **Configuration** B

In this configuration, the complex random vector $\mathbf{Y}_{R_b} = \mathbf{\Lambda}_{\sqrt{P_S}}\mathbf{\Lambda}_{\mathbf{H}_{SR_b}}\mathbf{X} + \mathbf{V}_{SR_b}$ models the symbol received by R_b node in the frequency domain. Adopting AF, the received symbol at D node is expressed as

$$\begin{aligned} \mathbf{Y}_D &= \mathbf{\Lambda}_{\sqrt{P_{R_b}}}\mathbf{\Lambda}^{-1/2}_{P_{\mathbf{Y}_{R_b}}}\mathbf{\Lambda}_{\mathbf{H}_{R_bD}}\mathbf{Y}_{R_b} + \mathbf{V}_{R_bD} \\ &= \mathbf{A}\mathbf{X} + \mathbf{B}\mathbf{V}, \end{aligned} \tag{2.9}$$

in which

$$\mathbf{A} = \mathbf{\Lambda}_{\sqrt{P_S}}\mathbf{\Lambda}_{\sqrt{P_{R_b}}}\mathbf{\Lambda}^{-1/2}_{P_{\mathbf{Y}_{R_b}}}\mathbf{\Lambda}_{\mathbf{H}_{SRb}}\mathbf{\Lambda}_{\mathbf{H}_{R_bD}}, \tag{2.10}$$

$$\mathbf{B} = [\mathbf{\Lambda}_{\sqrt{P_{R_b}}}\mathbf{\Lambda}^{-1/2}_{P_{\mathbf{Y}_{R_b}}}\mathbf{\Lambda}_{\mathbf{H}_{R_bD}} \quad \mathbf{I}_N], \tag{2.11}$$

$$\mathbf{V} = [\mathbf{V}_{SR_b}^T \mathbf{V}_{R_bD}^T]^T, \tag{2.12}$$

and $\mathbf{\Lambda}_{P_{\mathbf{Y}_{R_b}}} = \mathbf{\Lambda}_{P_S}\mathbf{\Lambda}_{|\mathbf{H}_{SR_b}|^2} + \mathbf{\Lambda}_{P_{\mathbf{V}_{SR_b}}}$ is the power vector associated with $\mathbf{Y}_{R_b}$. As a result, the SNR matrix associated with the use of the AF protocol is given by

$$\begin{aligned}
\mathbf{\Lambda}_{\gamma_{B,AF}} &\triangleq \mathbb{E}\{\mathbf{AX}(\mathbf{AX})^\dagger\}(\mathbb{E}\{\mathbf{BV}(\mathbf{BV})^\dagger\})^{-1} && (2.13)\\
&= \mathbf{A}\mathbf{R}_{\mathbf{XX}}\mathbf{A}^\dagger(\mathbf{B}\mathbf{R}_{\mathbf{VV}}\mathbf{B}^\dagger)^{-1} \\
&= \frac{\mathbf{\Lambda}_{P_S}\mathbf{\Lambda}_{P_{R_b}}\mathbf{\Lambda}_{P_{\mathbf{Y}_{R_b}}}^{-1}\mathbf{\Lambda}_{|\mathbf{H}_{SR_b}|^2}\mathbf{\Lambda}_{|\mathbf{H}_{R_bD}|^2}}{\mathbf{\Lambda}_{P_{R_b}}\mathbf{\Lambda}_{P_{\mathbf{Y}_{R_b}}}^{-1}\mathbf{\Lambda}_{|\mathbf{H}_{R_bD}|^2}\mathbf{\Lambda}_{P_{\mathbf{V}_{SR_b}}} + \mathbf{\Lambda}_{P_{\mathbf{V}_{R_bD}}}}. && (2.14)
\end{aligned}$$

Similarly to configuration A, the mutual information is given by

$$I(\mathbf{X};\mathbf{Y}_D) = \log_2[\det(\mathbf{I}_N + \mathbf{\Lambda}_{\gamma_{B,AF}})]. \tag{2.15}$$

Consequently, the ergodic achievable data rate for configuration B using the AF protocol can be expressed as

$$C_{B,AF} = \mathbb{E}_{\mathbf{H}}\left\{\max_{\mathbf{\Lambda}_{P_i}} \frac{B_w}{N\,N_T}\log_2[\det(\mathbf{I}_N + \mathbf{\Lambda}_{\gamma_{B,AF}})]\right\}, \tag{2.16}$$

subject to $\sum\limits_i \mathrm{Tr}(\mathbf{\Lambda}_{P_i}) \leq P$, with $i \in \{S, R_b\}$ and $N_T = 2$.

For DF protocol, it is assumed that R_b node is error-free, which means that this node can corretly decode all information received from S node and, as a consequence, simplifies the evaluation of the achievable data rate. Therefore, considering the maximum flow-minimum cut theorem [53], the ergodic achievable data rate for configuration B adopting DF is given by

$$C_{B,DF} = \mathbb{E}_{\mathbf{H}}\left\{\frac{1}{2}\min\{C_{SR_b}, C_{R_bD}\}\right\}, \tag{2.17}$$

where

$$C_{ij} = \max_{\mathbf{\Lambda}_{P_i}} \frac{B_w}{N\,N_T}\log_2[\det(\mathbf{I}_N + \mathbf{\Lambda}_{\gamma_{ij}})], \tag{2.18}$$

subject to $\sum\limits_i \mathrm{Tr}(\mathbf{\Lambda}_{P_i}) \leq P$, with $i \in \{S, R_a, R_b, R_c\}$, $j \in \{R_a, R_b, R_c, D\}$, and $N_T = 1$. The term $\frac{1}{2}$ in (2.17) is due to the presence of two transmitter nodes that use the channel during half of the available time interval (TDMA method).

2.2.3 Configurations C and D

Based on the fact that configurations C and D are SRC models [20], the functions $f_{AF}(\cdot)$ and $f_{DF}(\cdot)$ evaluate the achievable data rate of a SRC model using AF and DF, respectively (see Appendix A). Therefore, the ergodic achievable data rate for configurations

C and D can be expressed as

$$C_{C,AF} = \mathbb{E}_{\mathbf{H}} \left\{ f_{AF}(\mathcal{I}_{SD}, \mathcal{I}_{SR_a}, \mathcal{I}_{R_aD}) \right\}, \tag{2.19}$$

$$C_{C,DF} = \mathbb{E}_{\mathbf{H}} \left\{ f_{DF}(\mathcal{I}_{SD}, \mathcal{I}_{SR_a}, \mathcal{I}_{R_aD}) \right\}, \tag{2.20}$$

$$C_{D,AF} = \mathbb{E}_{\mathbf{H}} \left\{ f_{AF}(\mathcal{I}_{SD}, \mathcal{I}_{SR_c}, \mathcal{I}_{R_cD}) \right\}, \tag{2.21}$$

and

$$C_{D,DF} = \mathbb{E}_{\mathbf{H}} \left\{ f_{DF}(\mathcal{I}_{SD}, \mathcal{I}_{SR_c}, \mathcal{I}_{R_cD}) \right\}, \tag{2.22}$$

in which $\mathcal{I}_{ij}$ may denote $\mathbf{\Lambda}_{P_i}$, $\mathbf{\Lambda}_{|\mathbf{H}_{ij}|^2}$ and $\mathbf{\Lambda}_{P_{\mathbf{V}_{ij}}}$, in accord with the chosen configuration and cooperative protocol.

2.2.4 **Configuration** E

The mutual information between transmitted and received symbols in configuration E using AF is as follows:

$$I(\mathbf{X}; \mathbf{Y}_D) = \log_2[\det(\mathbf{I}_N + \mathbf{\Lambda}_{\gamma_{E,AF}})], \tag{2.23}$$

where $\mathbf{\Lambda}_{\gamma_{E,AF}}$ is deduced in Appendix B. Thus, the ergodic achievable data rate for configuration E using AF is given by

$$C_{E,AF} = \mathbb{E}_{\mathbf{H}} \left\{ \max_{\mathbf{\Lambda}_{P_i}} \frac{B_w}{N\, N_T} \log_2[\det(\mathbf{I}_N + \mathbf{\Lambda}_{\gamma_{E,AF}})] \right\}, \tag{2.24}$$

subject to $\sum\limits_{i} \mathrm{Tr}(\mathbf{\Lambda}_{P_i}) \leq P$, with $i \in \{S, R_a, R_b, R_c\}$ and $N_T = 4$.

Also, according to the maximum flow-minimum cut theorem and assuming that the relays are error-free, as in configuration B, the ergodic achievable data rate for configuration E using DF is expressed as

$$C_{E,DF} = \mathbb{E}_{\mathbf{H}} \left\{ \frac{1}{2} \min\{ f_{DF}(\mathcal{I}_{SR_b}, \mathcal{I}_{SR_a}, \mathcal{I}_{R_aR_b}), f_{DF}(\mathcal{I}_{R_bD}, \mathcal{I}_{R_bR_c}, \mathcal{I}_{R_cD}) \} \right\}, \tag{2.25}$$

in which the term $\frac{1}{2}$ is justified by the presence of two stages, as each one of them uses the channel during half of the available time interval.

2.3 SUMMARY

This chapter has focused on the 2S-SRC model and some of the most discussed cooperative channel models in the literature for improving the PLC system performance. Thus, the problem formulation addressing five configurations has been presented as well as

their ergodic achievable data rate expressions for both AF and DF cooperative protocols under the sum power constraint criterion and assuming the TDMA method to access the channel. MRC is used to signal combining.

3 HYBRID PLC/WIRELESS CHANNEL MODELS

The independent use of electric power grids and wireless media for data communication purpose has been pursued since long time ago. However, the need for maximizing their usage and fulfilling the astonishing and growing demands for connectivity among human beings and machines has brought attention to the drawbacks and limitations of these media. Attempting to address these issues, the investigation of the combined use of electric power grids and wireless media for data communication has started a few years ago. Currently, there is a great deal of attention in the parallel use of PLC and wireless channels to provide either reliability or high data rate, which has been called hybrid PLC/wireless data communication.

There are several works exploring the hybrid PLC/wireless data communication, but this topic may be complicated since the behavior of electric power grids for narrowband (frequency band from 0 up to 500 kHz) and broadband (frequency band from 1.7 up to 100 MHz) are different in terms of signal propagation and additive noise influence. And the same is applied to the wireless medium. In this regard, [30, 31, 33] addressed the narrowband hybrid PLC/wireless data communication, while [43–45] discussed general results related to PLC and wireless channels models. Moreover, there is a lack of contribution regarding broadband hybrid PLC/wireless data communication in the literature. As well as investigations for narrowband hybrid PLC/wireless data communication, works related to broadband hybrid PLC/wireless data communication are not simple since the scope and coverage must be clearly defined. With respect to only the PLC side, it is important to pay attention to the voltage level (low-, medium- and high-voltage), the type of environment, such as indoor (vehicle, residences and building) and outdoor (metropolitan and rural areas), among other issues. Bringing the wireless side to the discussion, other issues have to be addresses, such as the frequency bands and distances between nodes.

Based on the previous discussion, it is clear the need for correctly defining the frequency bands in which the hybrid PLC/wireless data communication is evaluated. In order to analyze the usefulness of the hybrid PLC/wireless data communication for broadband applications, this chapter focuses on hybrid channel models regarding a frequency band around 100 MHz. Driving the attention to one-hop links, only hybrid channel models in which the direct link is existing are analyzed in this chapter. By considering the frequency selectivity of both PLC and wireless channels, [48, 49] are used to derive the ergodic achievable data rates.

This chapter is organized as follows: Section 3.1 addresses the problem formulation and outlines the hybrid PLC/wireless channel models adopted in this chapter. Section 3.2 derives the ergodic achievable data rates for these models and Section 3.3 presents a succinct summary about this chapter.

3.1 PROBLEM FORMULATION

Two hybrid channel models for data communication purposes are adopted in this chapter (see Fig. 3). The first one does not consider the presence of active relays between S and D nodes and, as a consequence, it is named the hybrid one-hop channel (HOHC) model. This channel model was considered in previous works [43–46]. The second one is named the hybrid single-relay channel (HSRC) model and assumes that there is an active relay (R node) between S and D nodes, see details in [30, 31, 33]. In both models, all nodes can perform data communication over electric power grids and wireless media. In this work, the same symbols are transmitted through PLC and wireless channels by S and R nodes, which means that these channels are simultaneously accessed and the data communication aims to increase the reliability, coverage, and data rate. Based on the adoption of the TDMA method to access the channel, in the HSRC model, S node broadcasts the original information to R and D nodes, in the first time slot, while in the second one, R node forwards the information to D node.

Let the symbol transmitted by S node, in the frequency domain, be a Gaussian random vector given by $\mathbf{X} \in \mathbb{C}^{N\times 1}$, such that $\mathbb{E}\{\mathbf{X}\} = \mathbf{0}_{1\times N}$, $\mathbf{R}_{\mathbf{XX}} = \mathbb{E}\{\mathbf{X}\mathbf{X}^{\dagger}\} = N\mathbf{I}_N$. Also, $T_C^{\max} \gg T_S$, where $T_C^{\max}$ denotes the maximum coherence time considering both PLC and wireless channels and T_S is the symbol time interval (duration). Moreover, both PLC and wireless channels are modeled as LTI within a symbol time interval and the vectors representing the CIR of these channels are expressed as $\mathbf{h}_l^q = [h_l^q[1]\ h_l^q[2]\ ...\ h_l^q[L_l^q]]^T$, where L_l^q is the channel length, $q \in \{p, w\}$ indicates the medium (power line or wireless), and $l \in$

(a)

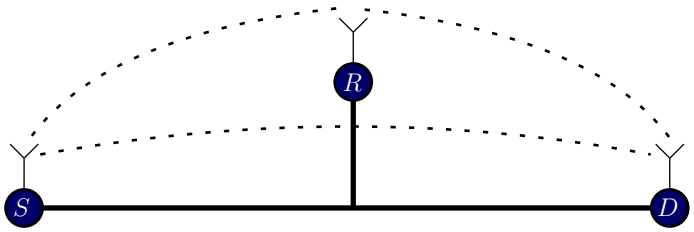

(b)

Figure 3: Adopted hybrid channel models. (a) HOHC model and (b) HSRC model.

$\{SD, SR, RD\}$ denotes the links source-destination, source-relay, and relay-destination, respectively. In addition, the N-length vector that represents the CFR of $\mathbf{h}_l^q$ is $\mathbf{H}_l^q = \mathbf{W}_N\ [\mathbf{h}_l^q\ \ \mathbf{0}_{1\times N-l}]^T$ and the diagonal matrices $\mathbf{\Lambda}_{\mathbf{H}_l}^q \triangleq \mathbf{diag}\{H_l^q[1], H_l^q[2], ..., H_l^q[N]\}$ and $\mathbf{\Lambda}_{|\mathbf{H}_l|^2}^q \triangleq \mathbf{diag}\{|H_l^q[1]|^2, |H_l^q[2]|^2, ..., |H_l^q[N]|^2\}$, in which $H_l^q[k]$ represents the k-th element of $\mathbf{H}_l^q$ $(k = 1, 2, ..., N)$.

Regarding the noise influence, let the additive noise at the output of the channel associated with the l link and q medium be represented by the Gaussian random vector $\mathbf{V}_l^q \in \mathbb{C}^{N\times 1}$, in the frequency domain, such that $\mathbb{E}\{\mathbf{V}_l^q\} = \mathbf{0}$, $\mathbb{E}\{\mathbf{V}_l^q \odot \mathbf{V}_j^q\} = \mathbb{E}\{\mathbf{V}_l^q\} \odot \mathbb{E}\{\mathbf{V}_j^q\}$, $\forall\ l \neq j$ and $j \in \{SD, SR, RD\}$. Also, $\mathbb{E}\{\mathbf{V}_l^p \odot \mathbf{V}_j^w\} = \mathbb{E}\{\mathbf{V}_l^p\} \odot \mathbb{E}\{\mathbf{V}_j^w\}$, $\forall j \in \{SD, SR, RD\}$ and $\mathbb{E}\{\mathbf{V}_l^q\mathbf{V}_l^q\dagger\} = N\mathbf{\Lambda}_{P_{\mathbf{V}_l^q}}$, in which $\mathbf{\Lambda}_{P_{\mathbf{V}_l^q}} \triangleq \mathbf{diag}\{P_{\mathbf{V}_l^q}[1], P_{\mathbf{V}_l^q}[2], ..., P_{\mathbf{V}_l^q}[N]\}$ and $P_{\mathbf{V}_l^q}[k]$ denotes the power of the k-th element of $\mathbf{V}_l^q$. Next, let $P_S^q \geq 0$ and $P_R^q \geq 0$ be the transmission powers allocated to S and R nodes and $q \in \{p, w\}$ medium, respectively. Similar to Chapter 2, the sum power constraint criterion is satisfied as follows:

$$\sum_q (P_S^q + P_R^q) \leq P, \tag{3.1}$$

in which $P \geq 0$ is the total transmission power. Besides, $\mathbf{\Lambda}_{\sqrt{P_S^q}} \triangleq \mathbf{diag}\{\sqrt{P_S^q[1]}, \sqrt{P_S^q[2]}, ..., \sqrt{P_S^q[N]}\}$, $\mathbf{\Lambda}_{\sqrt{P_R^q}} \triangleq \mathbf{diag}\{\sqrt{P_R^q[1]}, \sqrt{P_R^q[2]}, ..., \sqrt{P_R^q[N]}\}$, $\mathbf{\Lambda}_{P_S^q} \triangleq \mathbf{diag}\{P_S^q[1], P_S^q[2], ..., P_S^q[N]\}$, and $\mathbf{\Lambda}_{P_S^q} \triangleq \mathbf{diag}\{P_R^q[1], P_R^q[2], ..., P_R^q[N]\}$, where $P_S^q[k] \geq 0$ and $P_R^q[k] \geq 0$ are the power allocated to k-th subchannel and q medium at S and R nodes, respectively.

Based on the aforementioned formulation, the following questions arise: "Would a hybrid channel model benefit data communication between source and destination nodes when an in-home broadband data communication system is considered?", "Which one of the aforementioned hybrid channel models can achieve the highest ergodic achievable data rate when representative CFR and additive noise are applied?" In order to answer these interesting questions, Section 3.2 formulates ergodic achievable data rate expressions for these models.

3.2 ERGODIC ACHIEVABLE DATA RATE

This section aims to present the ergodic achievable data rate expressions for the adopted hybrid channel models. Such expressions will address the lack of combination as well as its presence at the destination node. The adopted roadmap aims to show the difference between both approaches when hybrid channel models are addressed. Regarding the HSRC model, the relay node adopts AF protocol and MRC technique to combine the received signals at the output of the PLC and wireless channels and the destination node also applies MRC technique for this purpose. This chapter only addresses the use of

the AF protocol and the MRC technique because the former is quite considered as the typical cooperative protocol to be analyzed and the latter yields the optimal performance in terms of signal combining. Moreover, the additive noise is a circularly-symmetric Gaussian random vector. Note that the additive noise is white in the wireless side while it is colored in the PLC side.

Furthermore, similar to Chapter 2 and [30, 31, 33], the use of LGRC [48, 49] is taken into account to deal with the inter-block interference created by PLC colored noise. Based on the fact that the adopted hybrid channel models have finite memory $L_{\max}$, in which $L_{\max} \geq \max_{l,q}\{L_l^q\}$ and $N \to \infty$, the achievable data rate of the adopted models can be approximated to that of N-CGRC.

3.2.1 Hybrid One-Hop Channel Model

First of all, let $\mathbf{Y}^p$ and $\mathbf{Y}^w$ be complex random vectors that represent the received signals at D node through power line and wireless media, respectively. Thus, the complex random vector that models the received symbol by D node is given by

$$\begin{aligned}
\mathbf{Y}' &= \begin{bmatrix} \mathbf{Y}^p \\ \mathbf{Y}^w \end{bmatrix} \\
&= \begin{bmatrix} \mathbf{\Lambda}_{\sqrt{P_S^p}\mathbf{\Lambda}_{\mathbf{H}_{SD}^p}}\mathbf{X} + \mathbf{V}_{SD}^p \\ \mathbf{\Lambda}_{\sqrt{P_S^w}\mathbf{\Lambda}_{\mathbf{H}_{SD}^w}}\mathbf{X} + \mathbf{V}_{SD}^w \end{bmatrix} \\
&= \begin{bmatrix} \mathbf{\Lambda}_{\sqrt{P_S^p}\mathbf{\Lambda}_{\mathbf{H}_{SD}^p}} & \mathbf{0}_{N\times N} \\ \mathbf{0}_{N\times N} & \mathbf{\Lambda}_{\sqrt{P_S^w}\mathbf{\Lambda}_{\mathbf{H}_{SD}^w}} \end{bmatrix} \begin{bmatrix} \mathbf{X} \\ \mathbf{X} \end{bmatrix} + \begin{bmatrix} \mathbf{V}_{SD}^p \\ \mathbf{V}_{SD}^w \end{bmatrix} \\
&= \mathbf{A}_{\mathbf{1}}'\mathbf{X}_{\mathbf{1}}' + \mathbf{V}_{\mathbf{1}}', \qquad (3.2)
\end{aligned}$$

in which

$$\mathbf{A}_{\mathbf{1}}' = \begin{bmatrix} \mathbf{\Lambda}_{\sqrt{P_S^p}\mathbf{\Lambda}_{\mathbf{H}_{SD}^p}} & \mathbf{0}_{N\times N} \\ \mathbf{0}_{N\times N} & \mathbf{\Lambda}_{\sqrt{P_S^w}\mathbf{\Lambda}_{\mathbf{H}_{SD}^w}} \end{bmatrix}, \qquad (3.3)$$

$\mathbf{V}_{\mathbf{1}}' = [\mathbf{V}_{SD}^p\ \mathbf{V}_{SD}^w]^T$, and $\mathbf{X}_{\mathbf{1}}' = [\mathbf{X}\ \mathbf{X}]^T$.

Without Combination: In this case, hardware complexity of D node is low and therefore it is not able to perform signal combining. It is assumed that the received signals from PLC and wireless channels are handled separately without considering a subsequent adoption of a combining technique (for more information on combining techniques, see [16]). Then, the resulting SNR matrix, without D node applying the combining technique, is expressed as

$$
\begin{aligned}
\boldsymbol{\Lambda}^{w/o}_{\gamma_{HOHC}} &= \mathbb{E}\{\mathbf{A}'_{\mathbf{1}}\mathbf{X}'_{\mathbf{1}}(\mathbf{A}'_{\mathbf{1}}\mathbf{X}'_{\mathbf{1}})^{\dagger}\}(\mathbb{E}\{\mathbf{V}'_{\mathbf{1}}{\mathbf{V}'_{\mathbf{1}}}^{\dagger}\})^{-1} \\
&= \mathbf{A}'_{\mathbf{1}}{\mathbf{R}_{\mathbf{X}'_{\mathbf{1}}\mathbf{X}'_{\mathbf{1}}}\mathbf{A}'_{\mathbf{1}}}^{\dagger}(\mathbf{R}_{\mathbf{V}'_{\mathbf{1}}\mathbf{V}'_{\mathbf{1}}})^{-1} \\
&= \begin{bmatrix} \boldsymbol{\Lambda}_{P_S^p}\boldsymbol{\Lambda}_{|\mathbf{H}^p_{SD}|^2} & \mathbf{0}_{N\times N} \\ \mathbf{0}_{N\times N} & \boldsymbol{\Lambda}_{P_S^w}\boldsymbol{\Lambda}_{|\mathbf{H}^w_{SD}|^2} \end{bmatrix} \begin{bmatrix} \boldsymbol{\Lambda}_{P_{\mathbf{V}^p_{SD}}} & \mathbf{0}_{N\times N} \\ \mathbf{0}_{N\times N} & \boldsymbol{\Lambda}_{P_{\mathbf{V}^w_{SD}}} \end{bmatrix}^{-1} \\
&= \begin{bmatrix} \dfrac{\boldsymbol{\Lambda}_{P_S^p}\boldsymbol{\Lambda}_{|\mathbf{H}^p_{SD}|^2}}{\boldsymbol{\Lambda}_{P_{\mathbf{V}^p_{SD}}}} & \mathbf{0}_{N\times N} \\ \mathbf{0}_{N\times N} & \dfrac{\boldsymbol{\Lambda}_{P_S^w}\boldsymbol{\Lambda}_{|\mathbf{H}^w_{SD}|^2}}{\boldsymbol{\Lambda}_{P_{\mathbf{V}^w_{SD}}}} \end{bmatrix}.
\end{aligned} \tag{3.4}
$$

Note that the resulting SNR matrix is block diagonal and, as a consequence, it is composed of the SNR matrix of both media in the main diagonal. Therefore, the ergodic achievable data rate for the HOHC model is given by

$$
C^{w/o}_{HOHC} = \mathbb{E}_{\mathbf{H}}\left\{ \max_{\boldsymbol{\Lambda}_{P_S^q}} \frac{B_w}{N\,N_T}\log_2[\det(\mathbf{I}_{2N} + \boldsymbol{\Lambda}^{w/o}_{\gamma_{HOHC}})] \right\}, \tag{3.5}
$$

subject to $\sum\limits_{q}\mathrm{Tr}(\boldsymbol{\Lambda}_{P_S^q}) \leq P$, with $q \in \{p, w\}$ and $N_T = 1$.

With Combination: From $\mathbf{Y}'$, given by (3.2), and weight matrices, $\mathbf{D}^q_{SD}$, the complex random vector that models the received symbol at D node in the frequency domain and after the use of the combining technique is given by

$$
\begin{aligned}
\mathbf{Y} &= \begin{bmatrix} \mathbf{D}^p_{SD} & \mathbf{D}^w_{SD} \end{bmatrix}\mathbf{Y}' \\
&= \mathbf{D}^p_{SD}\mathbf{Y}^p + \mathbf{D}^w_{SD}\mathbf{Y}^w \\
&= (\mathbf{D}^p_{SD}\boldsymbol{\Lambda}_{\sqrt{P_S^p}}\boldsymbol{\Lambda}_{\mathbf{H}^p_{SD}} + \mathbf{D}^w_{SD}\boldsymbol{\Lambda}_{\sqrt{P_S^w}}\boldsymbol{\Lambda}_{\mathbf{H}^w_{SD}})\mathbf{X} + (\mathbf{D}^p_{SD}\mathbf{V}^p_{SD} + \mathbf{D}^w_{SD}\mathbf{V}^w_{SD}) \\
&= \mathbf{A_1}\mathbf{X} + \mathbf{V_1},
\end{aligned} \tag{3.6}
$$

where $\mathbf{A_1} = \mathbf{D}^p_{SD}\boldsymbol{\Lambda}_{\sqrt{P_S^p}}\boldsymbol{\Lambda}_{\mathbf{H}^p_{SD}} + \mathbf{D}^w_{SD}\boldsymbol{\Lambda}_{\sqrt{P_S^w}}\boldsymbol{\Lambda}_{\mathbf{H}^w_{SD}}$ and $\mathbf{V_1} = \mathbf{D}^p_{SD}\mathbf{V}^p_{SD} + \mathbf{D}^w_{SD}\mathbf{V}^w_{SD}$. As a consequence, the resulting SNR matrix after the use of the combining technique is given by

$$
\begin{aligned}
\boldsymbol{\Lambda}^{w/}_{\gamma_{HOHC}} &= \mathbb{E}\{\mathbf{A_1}\mathbf{X}(\mathbf{A_1}\mathbf{X})^{\dagger}\}(\mathbb{E}\{\mathbf{V_1}{\mathbf{V_1}}^{\dagger}\})^{-1} \\
&= \mathbf{A_1}{\mathbf{R}_{\mathbf{XX}}\mathbf{A_1}}^{\dagger}(\mathbf{R}_{\mathbf{V_1}\mathbf{V_1}})^{-1} \\
&= \frac{|\mathbf{D}^p_{SD}\boldsymbol{\Lambda}_{\sqrt{P_S^p}}\boldsymbol{\Lambda}_{\mathbf{H}^p_{SD}} + \mathbf{D}^w_{SD}\boldsymbol{\Lambda}_{\sqrt{P_S^w}}\boldsymbol{\Lambda}_{\mathbf{H}^w_{SD}}|^2}{|\mathbf{D}^p_{SD}|^2\boldsymbol{\Lambda}_{P_{\mathbf{V}^p_{SD}}} + |\mathbf{D}^w_{SD}|^2\boldsymbol{\Lambda}_{P_{\mathbf{V}^w_{SD}}}}.
\end{aligned} \tag{3.7}
$$

Assuming that the combining technique is MRC means that $\mathbf{D}^q_{SD} = \boldsymbol{\Lambda}_{\sqrt{P_S^q}}\boldsymbol{\Lambda}_{\mathbf{H}^{q\dagger}_{SD}}/\boldsymbol{\Lambda}_{P_{\mathbf{V}^q_{SD}}}$ and, as a consequence, the SNR matrix for the HOHC model is given by

$$
\boldsymbol{\Lambda}^{w/}_{\gamma_{HOHC}} = \frac{\boldsymbol{\Lambda}_{P_S^p}\boldsymbol{\Lambda}_{|\mathbf{H}^p_{SD}|^2}}{\boldsymbol{\Lambda}_{P_{\mathbf{V}^p_{SD}}}} + \frac{\boldsymbol{\Lambda}_{P_S^w}\boldsymbol{\Lambda}_{|\mathbf{H}^w_{SD}|^2}}{\boldsymbol{\Lambda}_{P_{\mathbf{V}^w_{SD}}}}, \tag{3.8}
$$

which is the weighted sum of the SNR matrices associated with both media. As a result, the ergodic achievable data rate for the HOHC model with MRC is given by

$$C_{HOHC}^{w/} = \mathbb{E}_{\mathbf{H}} \left\{ \max_{\mathbf{\Lambda}_{P_S^q}} \frac{B_w}{N\, N_T} \log_2[\det(\mathbf{I}_N + \mathbf{\Lambda}_{\gamma_{HOHC}}^{w/})] \right\}, \tag{3.9}$$

subject to $\sum_q \mathrm{Tr}(\mathbf{\Lambda}_{P_S^q}) \leq P$, with $q \in \{p, w\}$ and $N_T = 1$.

3.2.2 Hybrid Single-Relay Channel Model

In this hybrid channel model, S and R nodes sends their information through both PLC and wireless channels. Therefore, in order to obtain the SNR matrix with and without combination, the vectorial representation of the four signals received by D node must be found. Two of them are originated in S node and described in Section 3.2.1, see (3.2), while the others came from R node.

For describing the signals originated in R node, it is needed to use the random vector $\mathbf{Y}_R^q = \mathbf{\Lambda}_{\sqrt{P_S^q}} \mathbf{\Lambda}_{\mathbf{H}_{SR}^q} \mathbf{X} + \mathbf{V}_{SR}^q$ that represents the symbol received by R node during the first time slot and through the q medium. Thus, with the possession of weight matrices $\mathbf{D}_{SR}^p$ and $\mathbf{D}_{SR}^w$, which are derived by the adoption of the MRC technique, the vector that represents the symbol at R node after the use of the combining technique is expressed as

$$\begin{aligned} \mathbf{Y}_R &= \begin{bmatrix} \mathbf{D}_{SR}^p & \mathbf{D}_{SR}^w \end{bmatrix} \begin{bmatrix} \mathbf{Y}_R^p \\ \mathbf{Y}_R^w \end{bmatrix} \\ &= (\mathbf{D}_{SR}^p \mathbf{\Lambda}_{\sqrt{P_S^p}} \mathbf{\Lambda}_{\mathbf{H}_{SR}^p} + \mathbf{D}_{SR}^w \mathbf{\Lambda}_{\sqrt{P_S^w}} \mathbf{\Lambda}_{\mathbf{H}_{SR}^w}) \mathbf{X} + (\mathbf{D}_{SR}^p \mathbf{V}_{SR}^p + \mathbf{D}_{SR}^w \mathbf{V}_{SR}^w) \\ &= \mathbf{A}_{\mathbf{2}}' \mathbf{X} + \mathbf{V}_{\mathbf{2}}', \end{aligned} \tag{3.10}$$

where $\mathbf{A}_{\mathbf{2}}' = \mathbf{D}_{SR}^p \mathbf{\Lambda}_{\sqrt{P_S^p}} \mathbf{\Lambda}_{\mathbf{H}_{SR}^p} + \mathbf{D}_{SR}^w \mathbf{\Lambda}_{\sqrt{P_S^w}} \mathbf{\Lambda}_{\mathbf{H}_{SR}^w}$ and $\mathbf{V}_{\mathbf{2}}' = \mathbf{D}_{SR}^p \mathbf{V}_{SR}^p + \mathbf{D}_{SR}^w \mathbf{V}_{SR}^w$.

In the sequel, the transmitted symbol from R node to D node is represented by $\mathbf{X}_R = \mathbf{\Lambda}_{P_{\mathbf{Y}_R}}^{-1/2} \mathbf{Y}_R$, in which $\mathbf{\Lambda}_{P_{\mathbf{Y}_R}} = \mathbb{E}\{\mathbf{Y}_R \mathbf{Y}_R^\dagger\}/N$ due to the adoption of the AF protocol. Hence, the received symbols by D node that was originated in R node are given by

$$
\begin{aligned}
\begin{bmatrix}\mathbf{Y}^p\\ \mathbf{Y}^w\end{bmatrix} &= \begin{bmatrix}\mathbf{\Lambda}_{\sqrt{P_R^p}}\mathbf{\Lambda}_{\mathbf{H}_{RD}^p}\mathbf{X}_R + \mathbf{V}_{RD}^p\\ \mathbf{\Lambda}_{\sqrt{P_R^w}}\mathbf{\Lambda}_{\mathbf{H}_{RD}^w}\mathbf{X}_R + \mathbf{V}_{RD}^w\end{bmatrix}\\
&= \begin{bmatrix}\mathbf{\Lambda}_{\sqrt{P_R^p}}\mathbf{\Lambda}_{\mathbf{H}_{RD}^p}[\mathbf{\Lambda}_{P_{\mathbf{Y}_R}}^{-1/2}(\mathbf{A_2'X} + \mathbf{V_2'})] + \mathbf{V}_{RD}^p\\ \mathbf{\Lambda}_{\sqrt{P_R^w}}\mathbf{\Lambda}_{\mathbf{H}_{RD}^w}[\mathbf{\Lambda}_{P_{\mathbf{Y}_R}}^{-1/2}(\mathbf{A_2'X} + \mathbf{V_2'})] + \mathbf{V}_{RD}^w\end{bmatrix}\\
&= \begin{bmatrix}\mathbf{\Lambda}_{\sqrt{P_R^p}}\mathbf{\Lambda}_{P_{\mathbf{Y}_R}}^{-1/2}\mathbf{\Lambda}_{\mathbf{H}_{RD}^p}\mathbf{A_2'} & \mathbf{0}_{N\times N}\\ \mathbf{0}_{N\times N} & \mathbf{\Lambda}_{\sqrt{P_R^w}}\mathbf{\Lambda}_{P_{\mathbf{Y}_R}}^{-1/2}\mathbf{\Lambda}_{\mathbf{H}_{RD}^w}\mathbf{A_2'}\end{bmatrix}\begin{bmatrix}\mathbf{X}\\ \mathbf{X}\end{bmatrix} +\\
&\quad \begin{bmatrix}\mathbf{\Lambda}_{\sqrt{P_R^p}}\mathbf{\Lambda}_{P_{\mathbf{Y}_R}}^{-1/2}\mathbf{\Lambda}_{\mathbf{H}_{RD}^p}\mathbf{V_2'} + \mathbf{V}_{RD}^p\\ \mathbf{\Lambda}_{\sqrt{P_R^w}}\mathbf{\Lambda}_{P_{\mathbf{Y}_R}}^{-1/2}\mathbf{\Lambda}_{\mathbf{H}_{RD}^w}\mathbf{V_2'} + \mathbf{V}_{RD}^w\end{bmatrix}.
\end{aligned}
\tag{3.11}
$$

As a result, the received symbol at D node considering the HSRC model is

$$
\begin{aligned}
\mathbf{Y'} &= \begin{bmatrix}\mathbf{\Lambda}_{\sqrt{P_S^p}}\mathbf{\Lambda}_{\mathbf{H}_{SD}^p} & \mathbf{0}_{N\times N} & \mathbf{0}_{N\times N} & \mathbf{0}_{N\times N}\\ \mathbf{0}_{N\times N} & \mathbf{\Lambda}_{\sqrt{P_R^p}}\mathbf{\Lambda}_{P_{\mathbf{Y}_R}}^{-1/2}\mathbf{\Lambda}_{\mathbf{H}_{RD}^p}\mathbf{A_2'} & \mathbf{0}_{N\times N} & \mathbf{0}_{N\times N}\\ \mathbf{0}_{N\times N} & \mathbf{0}_{N\times N} & \mathbf{\Lambda}_{\sqrt{P_S^w}}\mathbf{\Lambda}_{\mathbf{H}_{SD}^w} & \mathbf{0}_{N\times N}\\ \mathbf{0}_{N\times N} & \mathbf{0}_{N\times N} & \mathbf{0}_{N\times N} & \mathbf{\Lambda}_{\sqrt{P_R^w}}\mathbf{\Lambda}_{P_{\mathbf{Y}_R}}^{-1/2}\mathbf{\Lambda}_{\mathbf{H}_{RD}^w}\mathbf{A_2'}\end{bmatrix}\mathbf{X_2} +\\
&\quad + \begin{bmatrix}\mathbf{V}_{SD}^p\\ \mathbf{\Lambda}_{\sqrt{P_R^p}}\mathbf{\Lambda}_{P_{\mathbf{Y}_R}}^{-1/2}\mathbf{\Lambda}_{\mathbf{H}_{RD}^p}\mathbf{V_2'} + \mathbf{V}_{RD}^p\\ \mathbf{V}_{SD}^w\\ \mathbf{\Lambda}_{\sqrt{P_R^w}}\mathbf{\Lambda}_{P_{\mathbf{Y}_R}}^{-1/2}\mathbf{\Lambda}_{\mathbf{H}_{RD}^w}\mathbf{V_2'} + \mathbf{V}_{RD}^w\end{bmatrix}\\
&= \mathbf{A_2X_2} + \mathbf{V_2},
\end{aligned}
\tag{3.12}
$$

in which

$$
\mathbf{A_2} = \begin{bmatrix}\mathbf{\Lambda}_{\sqrt{P_S^p}}\mathbf{\Lambda}_{\mathbf{H}_{SD}^p} & \mathbf{0}_{N\times N} & \mathbf{0}_{N\times N} & \mathbf{0}_{N\times N}\\ \mathbf{0}_{N\times N} & \mathbf{\Lambda}_{\sqrt{P_R^p}}\mathbf{\Lambda}_{P_{\mathbf{Y}_R}}^{-1/2}\mathbf{\Lambda}_{\mathbf{H}_{RD}^p}\mathbf{A_2'} & \mathbf{0}_{N\times N} & \mathbf{0}_{N\times N}\\ \mathbf{0}_{N\times N} & \mathbf{0}_{N\times N} & \mathbf{\Lambda}_{\sqrt{P_S^w}}\mathbf{\Lambda}_{\mathbf{H}_{SD}^w} & \mathbf{0}_{N\times N}\\ \mathbf{0}_{N\times N} & \mathbf{0}_{N\times N} & \mathbf{0}_{N\times N} & \mathbf{\Lambda}_{\sqrt{P_R^w}}\mathbf{\Lambda}_{P_{\mathbf{Y}_R}}^{-1/2}\mathbf{\Lambda}_{\mathbf{H}_{RD}^w}\mathbf{A_2'}\end{bmatrix},
\tag{3.13}
$$

$$
\mathbf{V_2} = \begin{bmatrix}\mathbf{V}_{SD}^p\\ \mathbf{\Lambda}_{\sqrt{P_R^p}}\mathbf{\Lambda}_{P_{\mathbf{Y}_R}}^{-1/2}\mathbf{\Lambda}_{\mathbf{H}_{RD}^p}\mathbf{V_2'} + \mathbf{V}_{RD}^p\\ \mathbf{V}_{SD}^w\\ \mathbf{\Lambda}_{\sqrt{P_R^w}}\mathbf{\Lambda}_{P_{\mathbf{Y}_R}}^{-1/2}\mathbf{\Lambda}_{\mathbf{H}_{RD}^w}\mathbf{V_2'} + \mathbf{V}_{RD}^w\end{bmatrix},
\tag{3.14}
$$

and $\mathbf{X_2} = [\mathbf{X}\ \mathbf{X}\ \mathbf{X}\ \mathbf{X}]^T$.

Without Combination: Once more, the SNR matrix of the received symbol without combination must be found, see (3.17) on page 32. Then, the ergodic achievable data rate

for the HSRC model without combination is given by

$$C_{HSRC}^{w/o} = \mathbb{E}_{\mathbf{H}} \left\{ \max_{\mathbf{\Lambda}_{P_i^q}} \frac{B_w}{N\, N_T} \log_2[\det(\mathbf{I}_{4N} + \mathbf{\Lambda}_{\gamma_{HSRC}}^{w/o})] \right\}, \tag{3.15}$$

subject to $\sum_{i,q} \mathrm{Tr}(\mathbf{\Lambda}_{P_i^q}) \leq P$, with $i \in \{S, R\}$, $q \in \{p, w\}$, and $N_T = 2$.

With Combination: As in HOHC model, the SNR matrix for the HSRC model with combination, assuming that MRC is used, is equal to the sum of q media SNR matrices, see (3.18) on page 32. Therefore, the ergodic achievable data rate for the HSRC model after D node performs signal combining is given by

$$C_{HSRC}^{w/} = \mathbb{E}_{\mathbf{H}} \left\{ \max_{\mathbf{\Lambda}_{P_i^q}} \frac{B_w}{N\, N_T} \log_2[\det(\mathbf{I}_N + \mathbf{\Lambda}_{\gamma_{HSRC}}^{w/})] \right\}, \tag{3.16}$$

subject to $\sum_{i,q} \mathrm{Tr}(\mathbf{\Lambda}_{P_i^q}) \leq P$, with $i \in \{S, R\}$, $q \in \{p, w\}$, and $N_T = 2$.

3.3 SUMMARY

This chapter has concentrated on the HSRC and HOHC models. In this regard, it has presented the problem formulation related to these hybrid channel models and their ergodic achievable data rate expressions when the AF protocol applies together with or without signal combining at the destination node.

$$
\begin{aligned}
\mathbf{\Lambda}_{\gamma_{HSRC}}^{w/o} &= \mathbb{E}\{\mathbf{A_2 X_2}(\mathbf{A_2 X_2})^{\dagger}\}(\mathbb{E}\{\mathbf{V_2 V_2}^{\dagger}\})^{-1} \\
&= \mathbf{A_2 R_{X_2 X_2} A_2}^{\dagger}(\mathbf{R_{V_2 V_2}})^{-1} \\
&= \begin{bmatrix}
\frac{\mathbf{\Lambda}_{P_S^p}\mathbf{\Lambda}_{|\mathbf{H}_{SD}^p|^2}}{\mathbf{\Lambda}_{P_{\mathbf{V}_{SD}^p}}} & \mathbf{0}_{N\times N} & \mathbf{0}_{N\times N} & \mathbf{0}_{N\times N} \\
\mathbf{0}_{N\times N} & \frac{\mathbf{\Lambda}_{P_R^p}\mathbf{\Lambda}_{P_{\mathbf{Y}_R}}\mathbf{\Lambda}_{|\mathbf{H}_{RD}^p|^2|\mathbf{A_2'}|^2}}{\mathbf{\Lambda}_{P_R^p}\mathbf{\Lambda}_{P_{\mathbf{Y}_R}}\mathbf{\Lambda}_{|\mathbf{H}_{RD}^p|^2}\mathbf{\Lambda}_{P_{\mathbf{V'}_2}}+\mathbf{\Lambda}_{P_{\mathbf{V}_{RD}^p}}} & \mathbf{0}_{N\times N} & \mathbf{0}_{N\times N} \\
\mathbf{0}_{N\times N} & \mathbf{0}_{N\times N} & \frac{\mathbf{\Lambda}_{P_S^w}\mathbf{\Lambda}_{|\mathbf{H}_{SD}^w|^2}}{\mathbf{\Lambda}_{P_{\mathbf{V}_{SD}^w}}} & \mathbf{0}_{N\times N} \\
\mathbf{0}_{N\times N} & \mathbf{0}_{N\times N} & \mathbf{0}_{N\times N} & \frac{\mathbf{\Lambda}_{P_R^w}\mathbf{\Lambda}_{P_{\mathbf{Y}_R}}\mathbf{\Lambda}_{|\mathbf{H}_{RD}^w|^2|\mathbf{A_2'}|^2}}{\mathbf{\Lambda}_{P_R^w}\mathbf{\Lambda}_{P_{\mathbf{Y}_R}}\mathbf{\Lambda}_{|\mathbf{H}_{RD}^w|^2}\mathbf{\Lambda}_{P_{\mathbf{V'}_2}}+\mathbf{\Lambda}_{P_{\mathbf{V}_{RD}^w}}}
\end{bmatrix}
\end{aligned} \tag{3.17}
$$

where $\mathbf{\Lambda}_{P_{\mathbf{V'}_2}} = |\mathbf{D}_{SR}^p|^2\mathbf{\Lambda}_{P_{\mathbf{V}_{SR}^p}} + |\mathbf{D}_{SR}^w|^2\mathbf{\Lambda}_{P_{\mathbf{V}_{SR}^w}}$.

$$
\mathbf{\Lambda}_{\gamma_{HSRC}}^{w/} = \frac{\mathbf{\Lambda}_{P_S^p}\mathbf{\Lambda}_{|\mathbf{H}_{SD}^p|^2}}{\mathbf{\Lambda}_{P_{\mathbf{V}_{SD}^p}}} + \frac{\mathbf{\Lambda}_{P_R^p}\mathbf{\Lambda}_{P_{\mathbf{Y}_R}}\mathbf{\Lambda}_{|\mathbf{H}_{RD}^p|^2}|\mathbf{A_2'}|^2}{\mathbf{\Lambda}_{P_R^p}\mathbf{\Lambda}_{P_{\mathbf{Y}_R}}\mathbf{\Lambda}_{|\mathbf{H}_{RD}^p|^2}\mathbf{\Lambda}_{P_{\mathbf{V'}_2}} + \mathbf{\Lambda}_{P_{\mathbf{V}_{RD}^p}}} + \frac{\mathbf{\Lambda}_{P_S^w}\mathbf{\Lambda}_{|\mathbf{H}_{SD}^w|^2}}{\mathbf{\Lambda}_{P_{\mathbf{V}_{SD}^w}}} + \frac{\mathbf{\Lambda}_{P_R^w}\mathbf{\Lambda}_{P_{\mathbf{Y}_R}}\mathbf{\Lambda}_{|\mathbf{H}_{RD}^w|^2}|\mathbf{A_2'}|^2}{\mathbf{\Lambda}_{P_R^w}\mathbf{\Lambda}_{P_{\mathbf{Y}_R}}\mathbf{\Lambda}_{|\mathbf{H}_{RD}^w|^2}\mathbf{\Lambda}_{P_{\mathbf{V'}_2}} + \mathbf{\Lambda}_{P_{\mathbf{V}_{RD}^w}}}. \tag{3.18}
$$

4 NUMERICAL RESULTS

In this chapter, performance analyses for the ergodic achievable data rates presented in Chapters 2 and 3 are carried out. For this purpose, a data set of more than $30,000$ estimates of in-home PLC channels and several additive noise measurements are used. This data set was obtained from a measurement campaign detailed in [19,20], which considered seven residences, covering houses and apartments (in-home facilities), located in the urban area of the city of Juiz de Fora, Brazil.

This measurement campaign adopted the setup discussed in [6] and the methodology based on a hermitian-symmetric orthogonal frequency-division multiplexing (HS-OFDM) scheme reported in [54]. Also, it adopted a sampling frequency of 200 MHz; a frequency band (B_w) from 1.7 to 100 MHz; an HS-OFDM symbol length of $2N = 4096$; a symbol time interval of 23.04 μs; a frequency resolution of 48.8 kHz. Fig. 4 shows the noise power spectral density (PSD) of three of the additive noise measurements obtained from this measurement campaign.

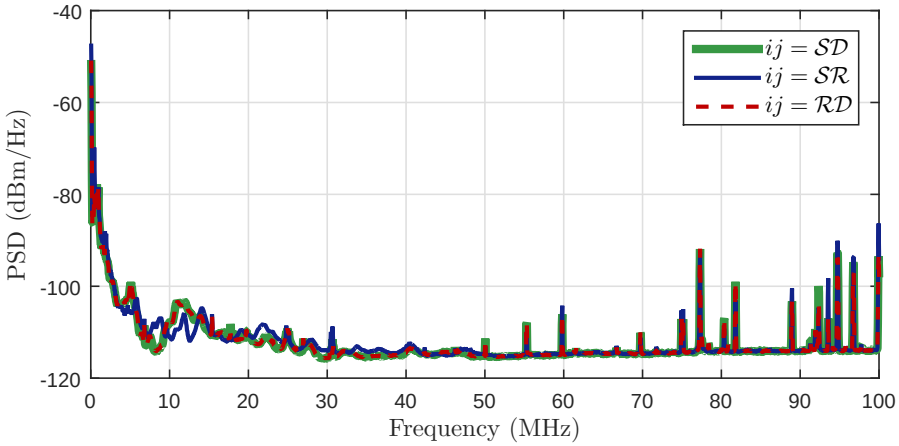

Figure 4: PSD of an additive noise measurement in $\mathcal{SD}$, $\mathcal{SR}$, and $\mathcal{RD}$ channels.

For wireless channel, the HIPERLAN/2 channel [55,56] is considered in this work. The HIPERLAN standard is a wireless local area network standard that has been defined by the European Telecommunications Standards Institute as an alternative to the IEEE 802.11 standards. The HIPERLAN second version [55,56], also known as HIPERLAN/2, has been developed within a standardization project for broadband radio access networks. This version has five channel models that operates in 5 GHz band and can be deployed in several environments, such as offices, exhibition halls, and industrial buildings. Among them, the first one is chosen because it has been developed for typical office environments under the assumption of non-line-of-sight propagation conditions. Its specifications are presented in Appendix C. According to that, the delay spread is equal to 50 ns, resulting in a frequency bandwidth equal to 20 MHz. To obtain a wireless channel with a

frequency bandwidth around to 100 MHz, this work considers a concatenation of five of these channels in the frequency domain.

For analyzing the performance of the hybrid and non-hybrid cooperative channel models under different relays positions, the data set of measured PLC channels is divided into four cases. To do so, let $\mathbf{h}^p_{\mathcal{SD}}$, $\mathbf{h}^p_{\mathcal{SR}}$ and $\mathbf{h}^p_{\mathcal{RD}}$ denote CIRs of a generic SRC model, then the energy ratios $\beta_1 \triangleq \frac{||\mathbf{h}^p_{\mathcal{SR}}||^2}{||\mathbf{h}^p_{\mathcal{SD}}||^2}$ and $\beta_2 \triangleq \frac{||\mathbf{h}^p_{\mathcal{RD}}||^2}{||\mathbf{h}^p_{\mathcal{SD}}||^2}$ (where $||\cdot||$ is the 2-norm of a vector) make possible to organize the cases as follows:

- Case #1: the relay is located halfway between source and destination nodes, resulting in $0.4\beta_1 \leq \beta_2 \leq 2.5\beta_1$ and $\beta_1^2 + \beta_2^2 \geq 1$.
- Case #2: the relay is closer to the destination node than to the source node, resulting in $2.5\beta_1 \leq \beta_2$ and $\beta_1^2 + \beta_2^2 \geq 1$.
- Case #3: the relay is closer to the source node than to the destination node, resulting in $0.4\beta_1 \geq \beta_2$ and $\beta_1^2 + \beta_2^2 \geq 1$.
- Case #4: the relay is far from both source and destination nodes, resulting in $\beta_1^2 + \beta_2^2 \leq 1$.

Fig. 5 shows these cases, representing all measured PLC channels in a $\beta_1 \times \beta_2$ plane in which the dashed lines symbolize the separation among the cases.

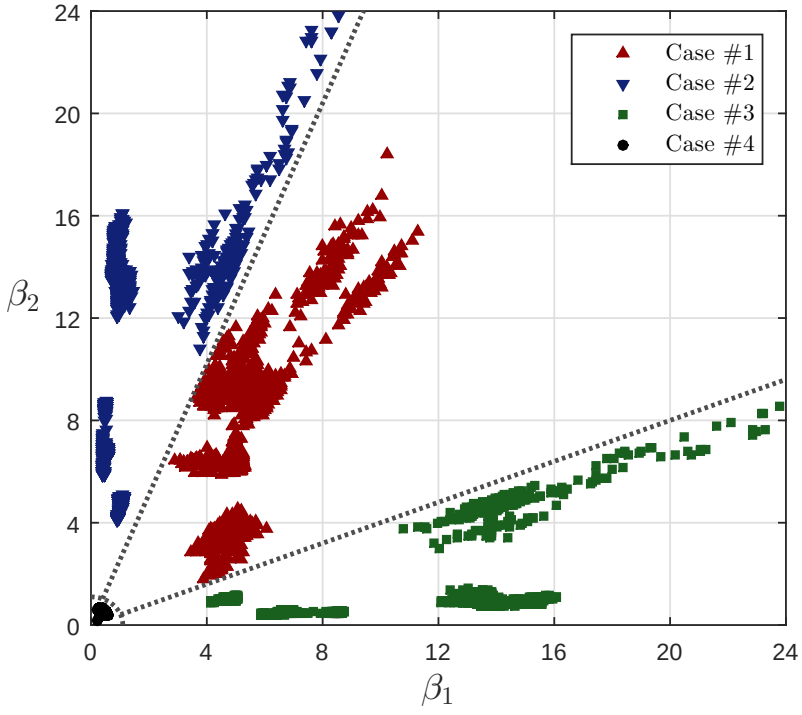

Figure 5: $\beta_1 \times \beta_2$ plane used to organize the data set in the four cases covered in [20].

The analyses presented in this chapter consider the total transmission power $P \in \{0, 10, 20, 30\}$ dBm since these values cover ranges of transmission power that are allowed to data communication systems in which the considered channel models operate.

4.1 TWO-STAGE SINGLE-RELAY CHANNEL MODEL

In this section, the numerical results for the five configurations discussed in Chapter 2 are presented in terms of ergodic achievable data rate gain, which is defined as follows:

$$\rho_{\alpha_1} \triangleq \frac{C_{\alpha_1,\alpha_2}}{C_A}, \tag{4.1}$$

where $\alpha_1 \in \{A, B, C, D, E\}$ refers to a configuration (see Fig. 2) and $\alpha_2 \in \{AF, DF\}$ is the cooperative protocol. Note that $C_A \in \{C_{A,AF}, C_{A,DF}\}$ in accord with the type of the cooperative protocol and, as a consequence, the ergodic achievable data rate gain of configuration A is always equal to unity since it is taken as reference. For evaluating how the channel conditions can influence the behavior of the 2S-SRC model, this work shows analyses for several average channel gain values of the $\mathbf{H}_{SD}$ ($G_{SD} = 10\log_{10}(1/N \sum_{k=1}^{N} |H_{SD}[k]|^2)$), while the PSD of the additive noise is always the same. This allow us to objectively evaluate the advantages and disadvantages of cooperative protocols when G_{SD} varies in a realistic range of values that are expected within a home.

In order to calculate the ergodic achievable data rates, one hundred events are used for each configuration and case. For every event, a pair of SRCs of the same case is randomly selected within the data set. The first SRC composes the channels h_{SR_b}, h_{SR_a}, and $h_{R_aR_b}$, while the second one forms the channels h_{R_bD}, $h_{R_bR_c}$, and h_{R_cD}. To constitute the adopted configurations, the channels of these two SRC are concatenated. As an example, to obtain the CIR between R_b and D nodes (used in configuration C), simply concatenate $h_{R_aR_b}$ and $h_{R_aR_b}$ channels, in other words, $h_{R_aD} = h_{R_aR_b} \star h_{R_bD}$, where $\star$ represents the convolution operator over two vectors.

Note that both configurations A and B are not influenced by the relays locations, since the first does not have active relay nodes and the second has just R_b node which stays invariably halfway between S and D nodes. An insight on what happens in configurations C and D for different cases can be provided by analyzing configuration E under absence of R_c and R_a nodes, respectively. Concerning configuration E, case #1 keeps R_a node close to S and R_b nodes, while R_c node is close to both R_b and D nodes. Case #2 places R_a and R_c nodes close to S and R_b nodes, respectively, whereas case #3 places R_a and R_c nodes close to R_b and D nodes. At last, case #4 keeps both R_a and R_c nodes away from S, R_b, and D nodes.

4.1.1 Ergodic Achievable Data Rate vs Total Transmission Power

As presented in [57], 90 % of PLC channel measurements in the frequency band from 1.7 to 100 MHz have average channel gain around -40 dB. As distances associated with two-hop links in in-home facilities are considered, the ergodic achievable data rates are presented considering $G_{SD} = -80$ dB, which is twice what is considered in [20], on average.

Fig. 6 shows the ergodic achievable data rate gains for the four analyzed cases when AF is adopted. Note that configuration B offers the best performance in terms of ergodic achievable data rate, always followed by configurations E, D, and C, in this order. It can also be noted that the gains are never greater than unity for configuration C and may vary significantly from case to case. For example, the ergodic achievable data rate gain for configuration B ranges from 2.1 up to 2.6 for case #1, while it ranges from 1.2 up to 1.8 for cases #2 and #3. If the set of P values covered higher values, it would be noticed that the ergodic achievable data rate gains tend to decrease along with P, which is not observed in Figs. 6b and 6c because the values of the adopted total transmission power are lower than 30 dBm. As considering such high P values would not be representative for practical systems, an initial instability in the curves causes intersections between them in Figs. 6b and 6c, masking the decreasing tendency of the achievable data rate gain along with P.

Moreover, the greatest gains have shown up in case #1. For instance, configuration B yields gains as higher as 2.5 times the reference. In addition, one can see that the worst gains appear in case #4, since only configuration B yields gains greater than unity and, as a consequence, the others configurations are not useful for enhancing the data communication between source and destination nodes. Regarding cases #1 and #4, all configurations shows a tendency to decrease the gains as the total transmission power increases, while in other cases it will depend upon the configuration. Additionally, it is expected that as P tends to infinity, the gains achieved by configurations C and D tend to $1/2$ since these configurations use the channel twice. Therefore, if the gain of one of these configurations is greater than unity for a given P and it starts to increase, then these gains decrease and, as a result, they become less than unity intersecting the reference. Because of this, ρ_D intersects ρ_A in Fig. 4a.

Analyzing cases #2 and #3, it is noticed that configurations C and D achieve gains lower than unity, which means that it is not worth exploring the diversity of these configurations in such cases. It somehow disagrees with [20] because the current work addresses distances corresponding to two-hop links. On the other hand, by analyzing configurations B and E, one can see that the gains can surpass more than 1.3 and 1.7, respectively. Furthermore, these configurations show similar gains in cases #2 and #3, which occurs due to the existing mirroring between these two cases in these configurations.

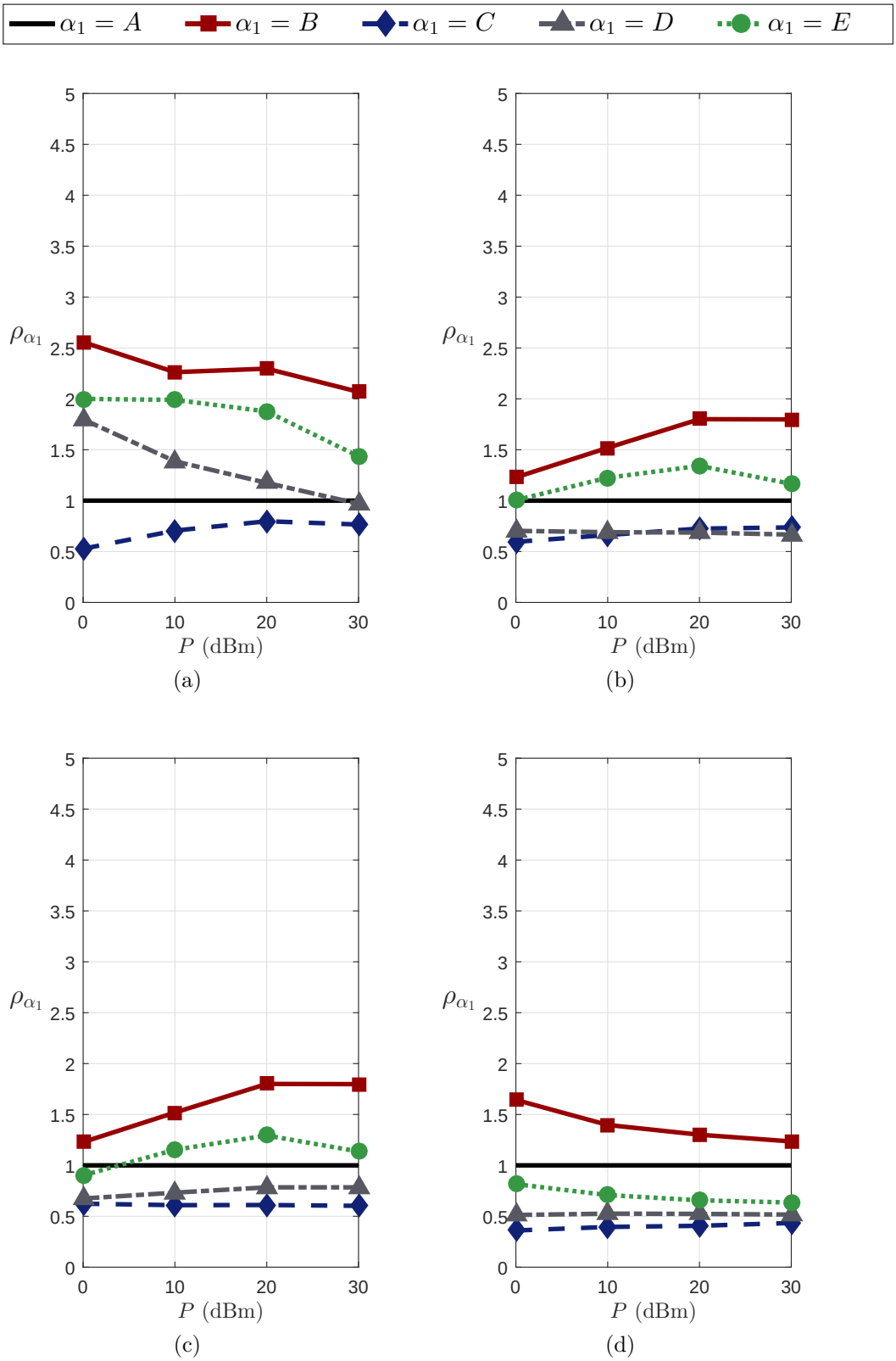

Figure 6: AF protocol and $G_{SD} = -80$ dB: Ergodic achievable data rate gain vs total transmission power. (a) case #1, (b) case #2, (c) case #3, and (d) case #4.

In fact, case #3 is obtained when S and D nodes positions changes in case #2 and vice versa.

Fig. 7 shows the ergodic achievable data rate gains associated with DF. First of all, DF achieves higher gains than AF and the gains decrease inversely along with total transmission power, as expected. In comparison to AF, the performance ranking remains the same among the analyzed configurations and cases #1, #2, and #3. As an exception, this ranking is altered in case #1, where configuration E exceeds configuration B for low values of P. This results in an intersection between the performance curves for these configurations and is explained as follows. Assuming DF protocol, configuration E yields superior performance compared to configuration B for low P values due to the presence of more active relays between source and destination nodes. These relays can eliminate the noise effect before the signal is greatly attenuated and, as the total transmission power increases, their presence becomes unnecessary, resulting in $\rho_B > \rho_E$.

Furthermore, as it occurs for AF, case #1 yields the best results while case #4 offers the worst ones. Focusing on case #1, one observes that the gains can reach high values mainly for configurations B and E. Besides, configuration C achieves significant gains, while configuration D does not achieve gains greater than unity. For case #4, configuration B is the only one that attains gains greater than unity. As the relays (represented by R_a and R_c nodes) are far from S and D nodes, configurations C, D, and E do not yield ergodic achievable data rate gains greater than unity for the considered values of P, as expected.

Now, turning our attention to cases #2 and #3, it can be seen that configurations B and E have quite similar gains due to the mirroring between them as previously discussed. In addition, the gains are greater than unity for configurations B and E in these cases, while they are smaller than unity for configurations C and D.

4.1.2 Ergodic Achievable Data Rate vs Average Channel Gain of the Direct Link

Overall, configurations B and E are the ones with the best performances in terms of ergodic achievable data rate. In addition, our results show that just for a specific situation (DF, case #1, $P = 0$ dBm) configuration E outperforms configuration B. However, it is our interest to evaluate whether this superiority occurs for different G_{SD} values. For this reason, an analysis of ρ_B/ρ_E ratio versus G_{SD} for distinct P values is carried out. If $\rho_B/\rho_E > 1$, then the ergodic achievable data rate achieved by configuration B is greater than the one achieved by configuration E, which means that it is better to use configuration B. On the other hand, if $\rho_B/\rho_E < 1$, then the opposite is valid. Based on the fact that the maximum and minimum average channel gain of in-home PLC channel are around -70 and -10 dB [57], respectively, and that two-hop links refer to

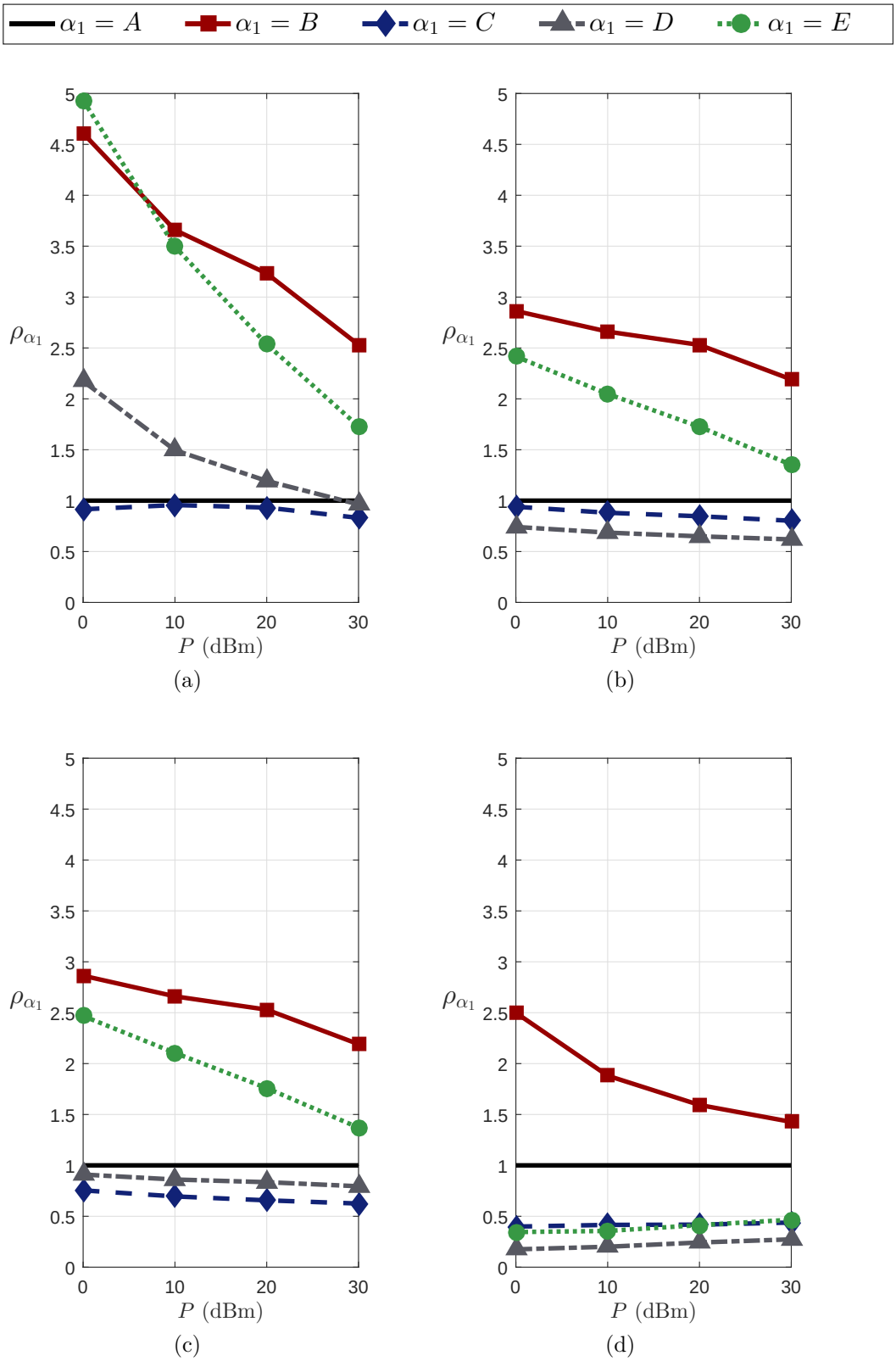

Figure 7: DF protocol and $G_{SD} = -80$ dB: Ergodic achievable data rate gain vs total transmission power. (a) case #1, (b) case #2, (c) case #3, and (d) case #4.

the concatenation of two PLC channels, this work considers G_{SD} values from -180 to -20 dB, i.e., twice the range from [57] with an extra margin for the lower bound.

Fig. 8 shows $\rho_B/\rho_E \times G_{SD}$ for distinct values of total transmission power when AF is adopted. It can be seen that the ergodic achievable data rate of configuration B tends to be twice the same of configuration E, as the direct link conditions improve ($G_{SD} \to 0$), which is due to the number of time slots of these configurations. Disregarding case #4 (Fig. 8.d), if the total transmission power is low, ρ_E tends to be greater than ρ_B more quickly as G_{SD} value decreases. To exemplify this statement, one can look at case #1 when $P = 0$ dBm and observe that configuration E is better than configuration B for $G_{SD} < -115$ dB, while for $P = 30$ dBm this just happens for $G_{SD} < -175$ dB. The same behavior is noticed in cases #2 and #3, but with a milder decrease in the value of ρ_B/ρ_E as G_{SD} decreases. Although all curves start very close to $G_{SD} = -20$ dB, the ρ_B/ρ_E ranges from 0.3 to 1.0 in case #1 and from 0.7 to 1.2 in cases #2 and #3 if $G_{SD} = -180$ dB.

A closer look at Fig. 8 shows that there is a range of G_{SD} values in which ρ_B/ρ_E remains approximately constant. Such behavior means that the performance ratio between configurations E and B remains constant within this interval of G_{SD}, i.e., the performances of configurations E and B vary at the same rate. It is important to say that, although the curves of different P apparently intersect each other, they portray distinct scenarios since they address different P values for a same noise PSD (see Fig. 4).

Regarding case #4, one first observes that, as the G_{SD} decreases, the value of ρ_B/ρ_E tends to be the same, unlike the previous cases. It means that no matter how much the average channel gain of the direct link decreases, configuration E is not better than configuration B, which confirms that the gains becomes less significant or even nonexistent, as the relays moves away from the direct link. In addition, such results clearly indicate how the use of TDMA method influences the ergodic achievable data rate gains. Due to the number of time slots, there is a reduction of 1/2 and 1/4 in the ergodic achievable data rates of configurations B and E, respectively. In conditions where there is no power allocated to R_a and R_c nodes, i.e., either direct link is not degraded or R_a and R_c nodes are far from the others, these reductions values are predominant in calculating the ρ_B/ρ_E ratio. Therefore, regardless the total transmission power, the ρ_B/ρ_E ratio is equal to 2 since configurations B and E use 2 and 4 time slots, respectively.

Fig. 9 shows ρ_B/ρ_E considering DF. For cases #1, #2, and #3, if the total transmission power is low, then ρ_B/ρ_E decreases more quickly as G_{SD} decreases, which is also observed if AF is adopted. Also, G_{SD} values at which $\rho_B/\rho_E = 1$ for DF are lower than they are for AF. For example, regarding case #1 and $P = 0$ and 30 dBm, these values are, respectively, equal to -75 and -135 dB for DF, i.e., 40 dB greater than what was observed for AF. By considering cases #2 and #3, one can observe that they

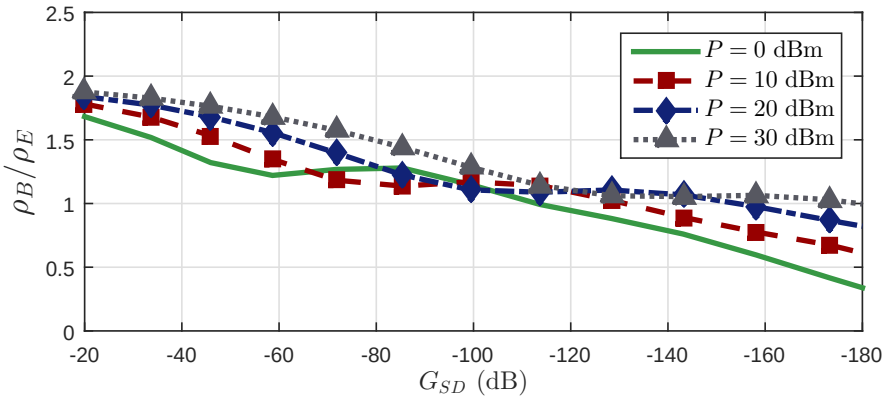

(a)

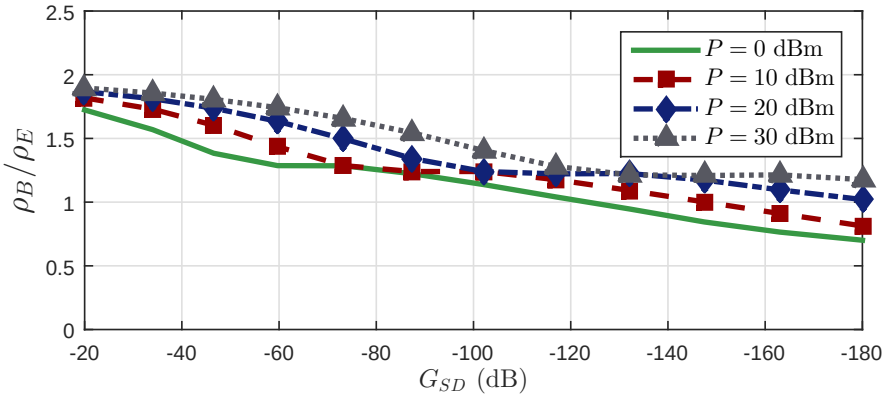

(b)

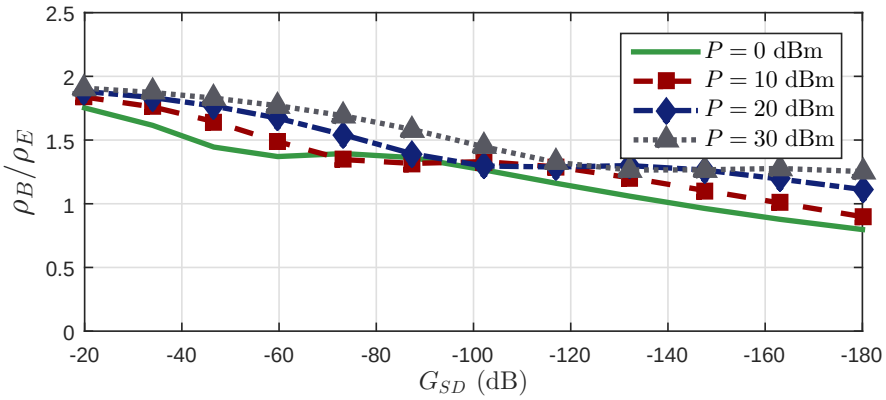

(c)

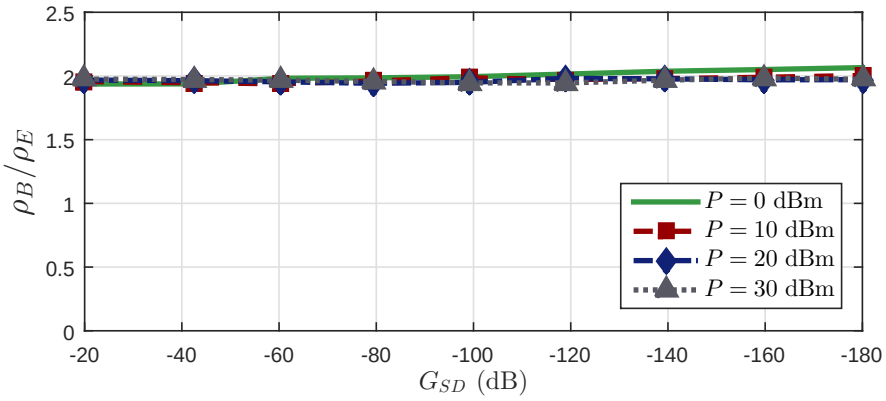

(d)

Figure 8: AF protocol and $\rho_B/\rho_E \times G_{SD}$. (a) case #1, (b) case #2, (c) case #3, and (d) case #4.

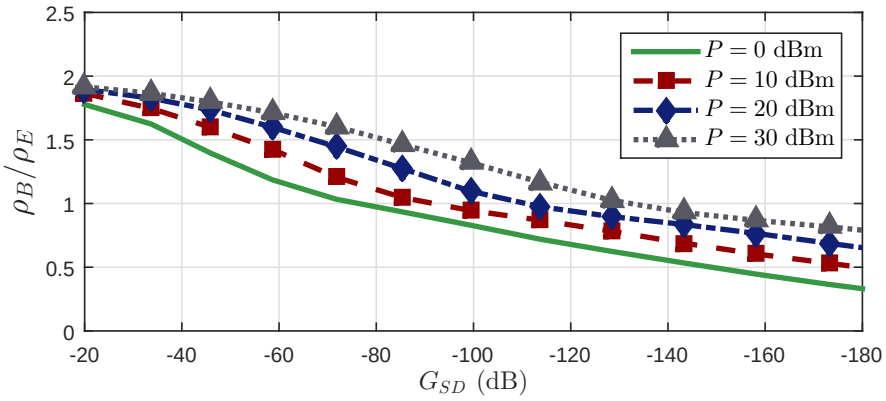

(a)

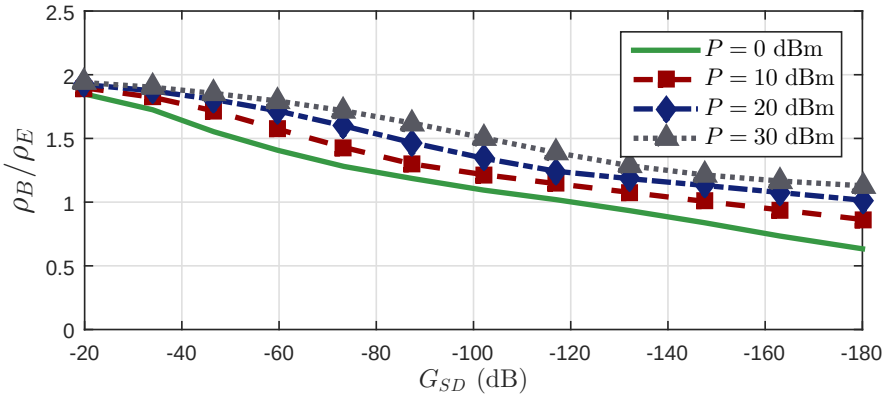

(b)

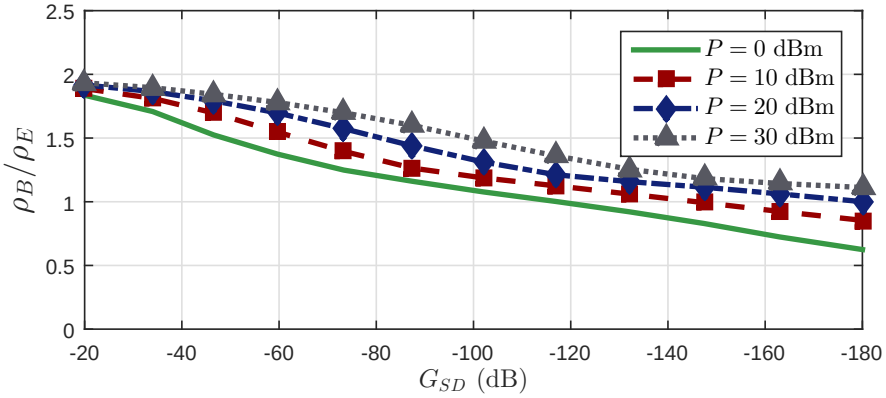

(c)

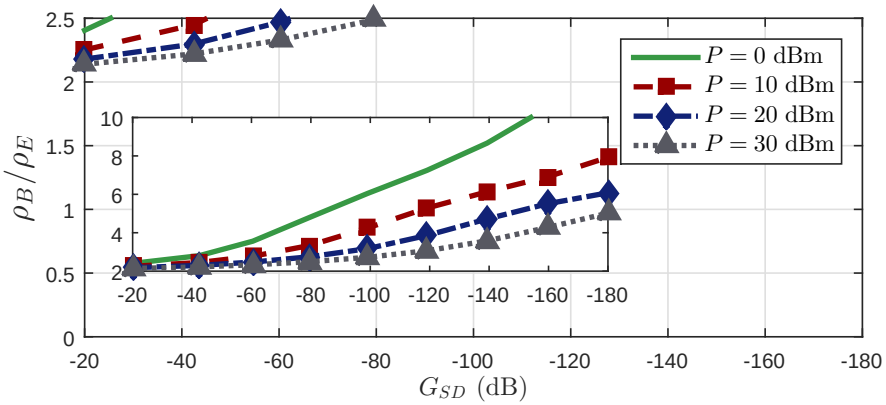

(d)

Figure 9: DF protocol and $\rho_B/\rho_E \times G_{SD}$. (a) case #1, (b) case #2, (c) case #3, and (d) case #4.

are quite similar, as the average channel gain values in which configuration B overcomes configuration E are the same in both cases (e.g. -120 and -150 dB for $P = 0$ and 10 dBm, respectively). A performance comparison in terms of the AF protocol shows that the ρ_B/ρ_E values are close to those for case #2 and a little smaller than that one for case #3.

Finally, case #4 behaves quite differently from the others cases. Actually, configuration E never offers a better performance than configuration B in terms of ergodic achievable data rate, since ρ_B/ρ_E is always greater than unity. Besides, if G_{SD} becomes smaller, then ρ_B/ρ_E tends towards infinity and, as P decreases, ρ_B/ρ_E tends to infinity more quickly.

4.2 HYBRID PLC/WIRELESS COOPERATIVE CHANNEL MODELS

This section shows the numerical results for the hybrid channel models described in Chapter 3. They are also presented in terms of ergodic achievable data rate gain, which is now defined as:

$$\rho_{\theta_1} \triangleq \frac{C_{\theta_1}^{\theta_2}}{C_{POHC}}, \tag{4.2}$$

where $\theta_1 \in \{POHC, WOHC, HOHC, PSRC, WSRC, HSRC\}$ indicates the analyzed channel models and $\theta_2 \in \{wi, wo\}$ refers to *with combination* and *without combination*, respectively. Note that, $C_{POHC}^{\theta_2}$, $C_{WOHC}^{\theta_2}$, $C_{PSRC}^{\theta_2}$, and $C_{WSRC}^{\theta_2}$ are obtained from their respective hybrid versions by making the total transmission power supplied to the other medium equal to zero, $C_{POHC}^{w/} = C_{POHC}^{w/o}$, and $C_{WOHC}^{w/} = C_{WOHC}^{w/o}$.

Again, one hundred events are used for each case; however, since this section does not consider two concatenated SRC models, each event is formed by only one SRC within the data set of the analyzed case. Moreover, in order to ensure fairness and evaluate only the diversity gain achieved by hybrid channel models, wireless channel energies are normalized by the PLC channel energies, i.e., for every event $||\mathbf{h}_l^w||^2 = ||\mathbf{h}_l^p||^2$. Given this normalization, wireless channel events will have the same ratio $\beta_1 \times \beta_2$ present in Fig. 5. Also, the noise in wireless communication is AWGN and its power is the same on PLC. Then, the PLC noise power is integrated in the considered frequency band and then equally divided in the wireless channel frequency band.

4.2.1 **Ergodic Achievable Data Rate Without Combination**

First of all, it is important to mention that distances associated with one-hop links for in-home broadband data communication are covered now and therefore ergodic achievable data rate gains assume that the average channel gain of the direct link is equal to -40 dB for PLC and wireless systems.

Fig. 10 shows ergodic achievable data rate gains for the four analyzed cases without signal combining at D node. It is first observed that HOHC and HSRC models present a superior performance in relation to their respective non-hybrid versions, i.e., one-hop channel and SRC using only PLC or wireless communication. One can notice that gains provided by the HSRC model may reach values close to three times the reference (case #1), while the ones provided by the HOHC model achieve more than twice the reference. Besides, it can be seen that, for all cases, the ergodic achievable data rate gains yielded by hybrid and wireless channel models show a increase tendency as the P value increases, while the PLC channel models depend upon the case.

Fig. 10 also shows that, except for case #4, there is different values of P in which $\rho_{POHC} = \rho_{WOHC}$ and $\rho_{PSRC} = \rho_{WSRC}$. At these points, both PLC and wireless models equally contribute to the gain yielded by the hybrid models. Hence, for low values of P, PLC channels are more relevant for the hybrid communication and, as the P value increases, wireless channels become more relevant. This result is somehow different from what was presented by [30], since PLC channels are always more relevant in [30].

Regarding the different results achieved by every model in each case, case #1 presents the best performances in terms of ergodic achievable data rate gain, followed by cases #2, #3, and #4, which again confirms that the relay is best used when it is halfway between source and destination nodes. Moreover, the HSRC model outperforms the HOHC model only in case #1, which means that, if the relay node is not located halfway between source and destination nodes, then the diversity gain introduced by the hybridism is enough. Also, it is worth mentioning that if the average channel gain of the direct link were lower than -40 dB, then different results could be observed.

4.2.2 **Ergodic Achievable Data Rate With Combination**

Fig. 11 presents ergodic achievable data rate gains for the four analyzed cases after D node performs combination. Once more, the best performances are yielded by the HOHC and HSRC models; however, less significant gains are now observed. For example, while the gains reached by the HSRC model may achieve values close to three times the reference *without combination*, they do not surpass twice the reference *with combination*. The fact that the hybrid system outperforms the best between wireless and PLC within the whole considered P range for both one-hop and single-relay channel models means that hybrid systems are capable of jointly exploiting the diversity of both PLC and wireless channels, therefore achieving better performance.

It is important to notice some similarities between both approaches, *with and without combination*. Firstly, it is worth remembering that the results for PLC and wireless one-hop channels are equal in both approaches. One can also observe that the HSRC model presents the best performance in case #1, while the HOHC model offers the

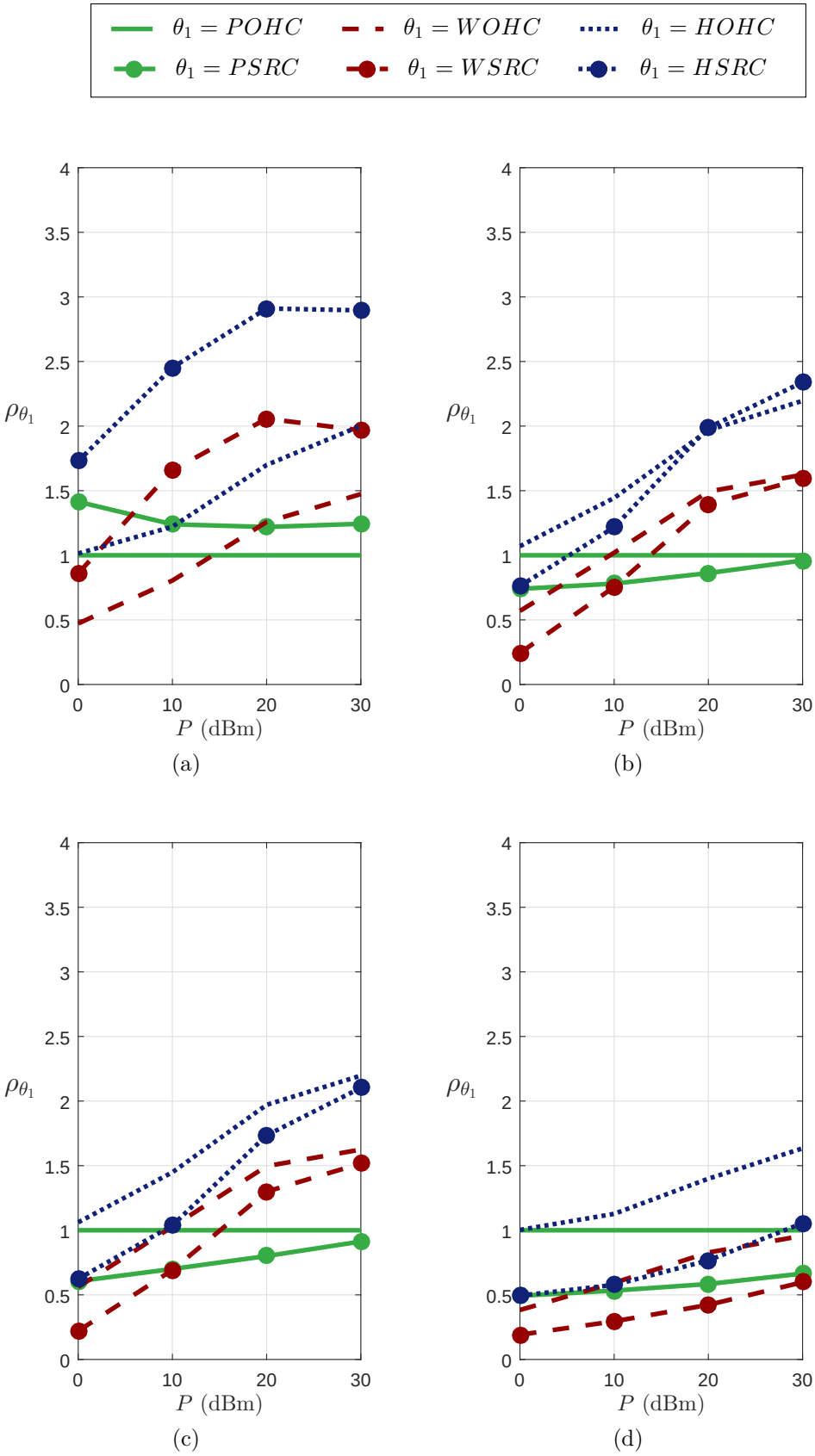

Figure 10: Without combination: Ergodic achievable data rate gain vs total transmission power. (a) case #1, (b) case #2, (c) case #3, and (d) case #4.

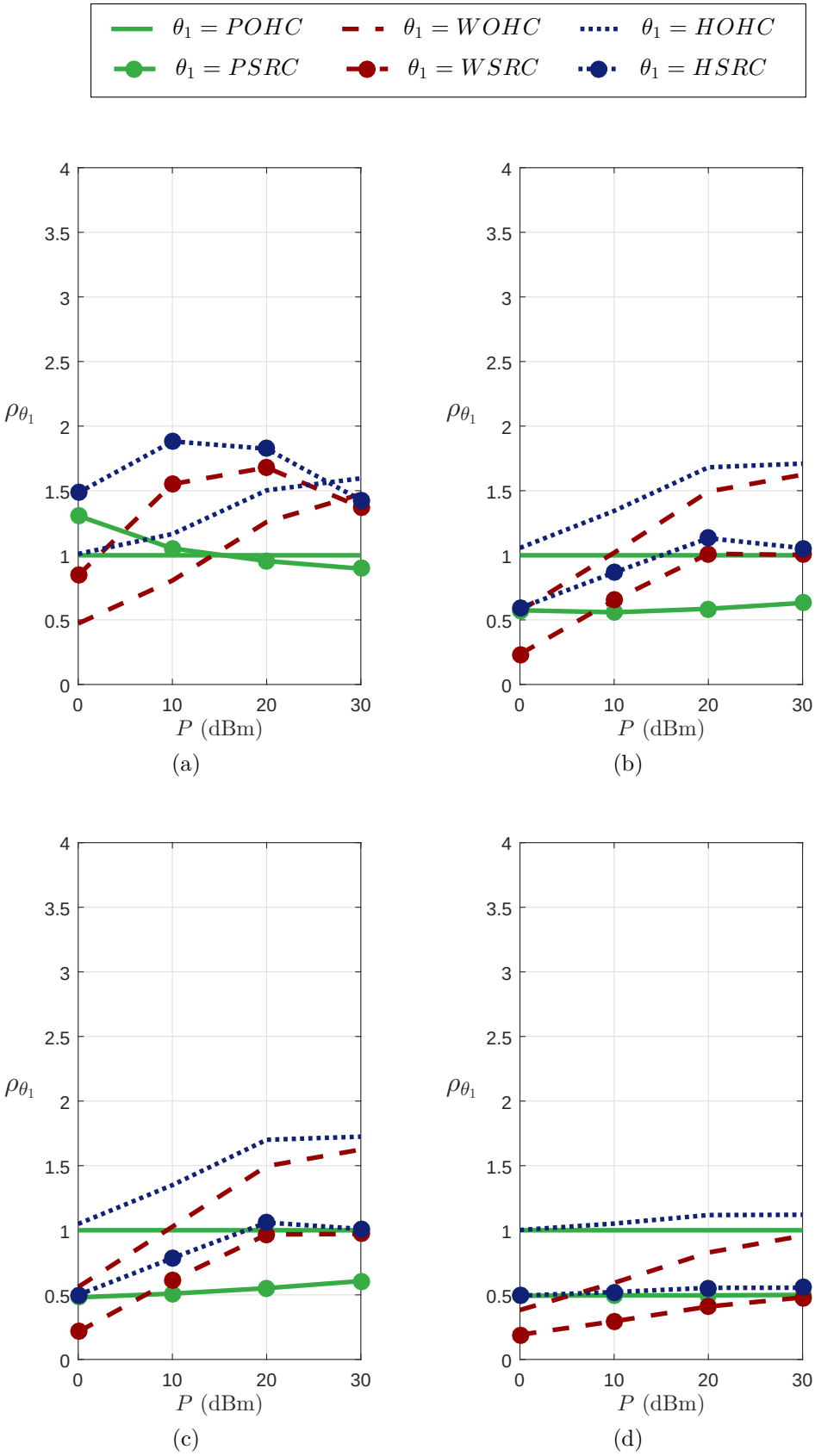

Figure 11: With combination: Ergodic achievable data rate gain vs total transmission power. (a) case #1, (b) case #2, (c) case #3, and (d) case #4.

greatest gains in cases #2, #3, and #4. Another similarity is related to the behavior of curves, i.e., the increase or decrease of gains as P increases.

Due to the number of time slots used for each model, ρ_{POHC}, ρ_{WOHC}, and ρ_{HOHC} tend to 1, while ρ_{PSRC}, ρ_{WSRC}, and ρ_{HSRC} tend to 1/2 as $P \to \infty$. This is quite clear in case #4. Nonetheless, PLC gains may increase, decrease, or even remain constant, depending on the case, while wireless and hybrid gains increase for low P values and then, as P increases, they stabilize. Hence, one can conclude that, if low P values are employed, then a hybrid system allocates more power to the PLC system. As higher P values are considered, the wireless system receives more power. Finally, as $P \to \infty$, both PLC and wireless systems yield similar performances.

4.3 SUMMARY

This chapter has presented several numerical analyses regarding Chapters 2 and 3. Ergodic achievable data rate results have been presented for different values of total transmission power and relative relays positions. Concerning Chapter 2, both AF and DF protocol have been employed as well as different average channel gain of the direct link. With respect to Chapter 3, the AF protocol and the MRC technique have been applied together with two approaches: with and without combination at the destination node.

5 CONCLUSIONS

In a nutshell, this work has discussed the usefulness of the 2S-SRC model for dealing with severely degraded source-to-destination links associated with in-home broadband PLC channels. Five configurations of this model that cover other types of well-known channel models, such as the one-hop channel model, the two-hop channel model, and the SRC model have been presented. Besides, ergodic achievable data rates by considering AF and DF with MRC have been derived and several analyses based on a data set constituted by measured PLC channels and additive noise covering the frequency band from 1.7 to 100 MHz have been carried out. These analyses have taken into account different relays positions, realistic total transmission powers and average channel gains of the direct link.

Furthermore, this work has analyzed the hybrid PLC/wireless SRC model for in-home broadband data communication systems. It has also investigated the hybrid one-hop channel model and presented comparative numerical analyses among hybrid and non-hybrid cooperative systems. In this regard, closed-form expressions for their ergodic achievable data rates by considering AF with MRC have been derived. For carrying out numerical analyses, the HIPERLAN/2 channel model corrupted by AWGN has been considered for wireless communication system. Additionally, relative relays positions and realistic total transmission powers have been employed.

Based on the obtained results, numerical analyses have shown that the higher the degradation imposed by the direct link, the better the 2S-SRC model in terms of ergodic achievable data rate, while the low level of degradation favors to the two-hop channel model. In addition, if the total transmission power is low, the two-hop channel model is quickly exceeded by the 2S-SRC model as the severity of degradation of the direct link increases. It has been concluded that the majority of cooperative channel models do not offer gains when the relay is far from both source and destination nodes. Also, the SRC model may be useless if the distance between source and destination nodes corresponds to two-hop links within a home. These surprising results indicate that cooperative communication associated with in-home broadband PLC systems may be more effective if either the 2S-SRC model or the two-hop channel model is adopted.

Moreover, it has shown that hybrid channel models can benefit data communication between source and destination nodes when a in-home broadband system is considered. Also, for distances corresponding to one-hop links, the HSRC model presents the best performance in terms of ergodic achievable data rate if the relay is halfway between source and destination nodes, while the HOHC model yields the best performance in other cases. Finally, this work has shown that the behavior of the ergodic achievable data rate with and without combination is similar, although the gains with combination are lower.

5.1 Future works

A list of future works is as follows:

- To investigate the complexity of the 2S-SRC model as well as other configurations from it.
- To analyze the ergodic achievable data rate for the HSRC model when the DF protocol applies at the relay node.
- To apply the broadband hybrid PLC/wireless data communication to other channel models, as the two-hop channel model.
- To expand these analyses to a hybrid system composed of PLC, wireless communication, and visible light communication.

REFERENCES

[1] L. T. Berger, A. Schwager, and J. J. E. Garzás, "Power line communications for smart grid applications," *Journal of Electrical and Computer Engineering*, vol. 2013, pp. 1–16, 2013.

[2] M. V. Ribeiro, G. R. Colen, F. V. P. D. Campos, Z. Quan, and H. V. Poor, "Clustered-orthogonal frequency division multiplexing for power line communication: when is it beneficial?" *IET Commun.*, vol. 8, no. 13, pp. 2336–2347, Sep. 2014.

[3] R. M. Oliveira, M. S. P. Facina, M. V. Ribeiro, and A. B. Vieira, "Performance evaluation of in-home broadband PLC systems using a cooperative mac protocol," *Computer Networks*, vol. 95, pp. 62–76, Dec. 2015.

[4] G. R. Colen, L. G. Oliveira, A. J. H. Vinck, and M. V. Ribeiro, "A spectral compressive resource allocation technique for PLC systems," *IEEE Trans. Commun.*, vol. 65, no. 2, pp. 816–826, Feb. 2017.

[5] L. G. de Oliveira, G. R. Colen, M. V. Ribeiro, and A. J. H. Vinck, "Narrow-band interference error correction in coded ofdm-based plc systems," in *2016 International Symposium on Power Line Communications and its Applications (ISPLC)*, Mar. 2016, pp. 13–18.

[6] G. R. Colen, C. A. G. Marques, T. R. Oliveira, F. P. V. de Campos, and M. V. Ribeiro, "Measurement setup for characterizing low-voltage and outdoor electric distribution grids for PLC systems," in *Proc. IEEE PES Conference On Innovative Smart Grid Technologies Latin America*, April 2013, pp. 1–5.

[7] A. Camponogara, T. R. Oliveira, W. A. Finamore, F. P. V. Campos, and M. V. Ribeiro, "Aircraft PLC channels characterization: Initial discussion," in *Proc. XXXIV Simpósio Brasileiro de Telecomunicações*, Sep. 2016, pp. 839–842.

[8] T. Rappaport, *Wireless Communications: Principles and Practice*, 2nd ed. Upper Saddle River, NJ, USA: Prentice Hall PTR, 2001.

[9] D. Tse and P. Viswanath, *Fundamentals of Wireless Communication*. New York, NY, USA: Cambridge University Press, 2005.

[10] A. Nosratinia, T. E. Hunter, and A. Hedayat, "Cooperative communication in wireless networks," *IEEE Commun. Mag*, vol. 42, no. 10, pp. 74–80, Oct. 2004.

[11] H. Hrasnica, A. Haidine, and R. Lehnert, *Broadband Powerline Communications: Network Design.* New York: John Wiley & Sons, 2005.

[12] S. Galli, A. Scaglione, and Z. Wang, "For the grid and through the grid: The role of power line communications in the smart grid," *Proc. IEEE*, vol. 99, no. 6, pp. 998–1027, Jun. 2011.

[13] A. A. M. Picorone, T. R. Oliveira, and M. V. Ribeiro, "PLC channel estimation based on pilots signal for OFDM modulation: A review," *IEEE Latin America Transactions*, vol. 12, no. 4, pp. 580–589, June 2014.

[14] G. R. Colen, L. G. de Oliveira, C. B. Zeller, A. J. Han Vinck, and M. V. Ribeiro, "Statistical analysis and modeling of a novel parameter for resource allocation in multicarrier PLC systems," *Trans. on Emerging Telecommun. Technologies*, vol. 28, no. 11, pp. 1–12, 2017.

[15] L. G. d. S. Costa, A. C. M. Queiroz, B. Adebisi, V. L. R. Costa, and M. V. Ribeiro, "Coupling for power line communications: A survey," *Journal of Commun. and Inf. Systems,*, vol. 32, no. 1, pp. 1–15, 2017.

[16] Y. P. Hong, W. Huang, and C. J. Kuo, *Cooperative Communications and Networking*. New York, NY, USA: Springer, 2010.

[17] M. Dohler and Y. Li, *Cooperative communications: hardware, channel & phy*. New York, NY, USA: John Wiley & Sons, 2010.

[18] I. Rubin, Y. Y. Lin, and D. Kofman, "Optimal relay configuration for power line communication networks," *IEEE Trans. Commun.*, vol. 64, no. 1, pp. 130–140, Jan 2016.

[19] J. Valencia, T. R. Oliveira, and M. V. Ribeiro, "Cooperative power line communication: Analysis of brazilian in-home channels," in *18th IEEE International Symposium on Power Line Communications and Its Applications*, March 2014, pp. 301–305.

[20] M. S. P. Facina, H. A. Latchman, H. V. Poor, and M. V. Ribeiro, "Cooperative in-home power line communication: analyses based on a measurement campaign," *IEEE Trans. Commun.*, vol. 64, no. 2, pp. 778–789, Feb. 2016.

[21] M. d. L. Filomeno, V. Fernandes, F. P. V. Campos, and M. V. Ribeiro, "Análise estatística da capacidade de canais plc residenciais cooperativos baseada no modelo single relay channel," in *Proc. XXXIV Simpósio Brasileiro de Telecomunicações*, Sep. 2016, pp. 843–847.

[22] M. Dong, W. Li, and F. Amirnavaei, "Online joint power control for two-hop wireless relay networks with energy harvesting," *IEEE Transactions on Signal Processing*, vol. 66, no. 2, pp. 463–478, Jan 2018.

[23] Y. Wu, L. P. Qian, L. Huang, and X. Shen, "Optimal relay selection and power control for energy-harvesting wireless relay networks," *IEEE Transactions on Green Communications and Networking*, vol. PP, no. 99, pp. 1–10, 2017.

[24] B. Li, Z. Fei, and H. Chen, "Robust artificial noise-aided secure beamforming in wireless-powered non-regenerative relay networks," *IEEE Access*, vol. 4, pp. 7921–7929, 2016.

[25] K. H. Kim, H. B. Lee, Y. H. Kim, J. H. Lee, and S. C. Kim, "Cooperative multihop AF relay protocol for medium-voltage power-line-access network," *IEEE Trans. Power Del.*, vol. 27, no. 1, pp. 195–204, Jan. 2012.

[26] A. Dubey and R. K. Mallik, "PLC system performance with AF relaying," *IEEE Trans. Commun.*, vol. 63, no. 6, pp. 2337–2345, Jun. 2015.

[27] X. Cheng, R. Cao, and L. Yang, "Relay-aided amplify-and-forward powerline communications," *IEEE Trans. Smart Grid*, vol. 4, no. 1, pp. 265–272, March 2013.

[28] A. Dubey, R. K. Mallik, and R. S. Schober, "Performance analysis of a multi-hop power line communication system over log-normal fading in presence of impulsive noise," *IET Commun.*, vol. 9, no. 1, pp. 1–9, 2015.

[29] N. Khyaria, S. Khalfallahb, Y. Barounib, and S. J. B. H., "Decode and forward relay-assisted power-line communication," *Procedia Computer Science*, vol. 73, pp. 209–216, 2015.

[30] V. Fernandes, W. A. Finamore, H. V. Poor, and M. V. Ribeiro, "The low-bit-rate hybrid power line/wireless single-relay channel," *IEEE Systems Journal*, vol. PP, no. 99, pp. 1–12, 2017.

[31] V. Fernandes, H. V. Poor, and M. V. Ribeiro, "Analyses of the incomplete low-bit-rate hybrid plc-wireless single-relay channel," *IEEE Internet of Things Journal*, vol. PP, no. 99, pp. 1–12, 2018.

[32] L. d. M. B. A. Dib, V. Fernandes, and M. V. Ribeiro, "A discussion about hybrid PLC-wireless communication for smart grids," in *Proc. XXXIV Simpósio Brasileiro de Telecomunicações*, Sep. 2016, pp. 848–852.

[33] L. de M. B. A. Dib, V. Fernandes, M. de L. Filomeno, and M. V. Ribeiro, "Hybrid PLC/wireless communication for smart grids and internet of things applications," *IEEE Internet of Things Journal*, vol. PP, no. 99, pp. 1–13, 2017.

[34] Y. H. Kim, S. Choi, S. C. Kim, and J. H. Lee, "Capacity of OFDM two-hop relaying systems for medium-voltage power-line access networks," *IEEE Trans. Power Del.*, vol. 27, no. 2, pp. 886–894, April 2012.

[35] K. M. Rabie, B. Adebisi, and A. Salem, "Improving energy efficiency in dual-hop cooperative PLC relaying systems," in *2016 International Symposium on Power Line Communications and its Applications (ISPLC)*, March 2016, pp. 196–200.

[36] X. Wu and Y. Rong, "Joint terminals and relay optimization for two-way power line information exchange systems with QoS constraints," *EURASIP journal on Advances in Signal Processing*, vol. 2015, no. 84, pp. 1–15, 2015.

[37] B. Nikfar and A. J. H. Vinck, "Relay selection in cooperative power line communication: A multi-armed bandit approach," *Journal of Communications and Networks*, vol. 19, no. 1, pp. 1–9, Feb. 2017.

[38] O. A. Gonzalez, J. Urminsky, M. Calvo, and L. de Haro, "Performance analysis of hybrid broadband access technologies using PLC and wi-fi," in *Proc. Int. Conf. on Wireless Netw., Commun. and Mobile Computing*, vol. 1, no. 12, Jun. 2005, pp. 564–569.

[39] T. Holden and J. Yazdani, "Hybrid security for hybrid vehicles exploring smart grid technology, powerline and wireless communication," in *Proc. IEEE PES Int. Conf. and Exhibition on Innov. Smart Grid Technol.*, Dec. 2011, pp. 1–5.

[40] A. Cataliotti *et al.*, "Experimental evaluation of an hybrid communication system architecture for smart grid applications," in *Proc. IEEE Int. Workshop on Applied Measurements for Power Systems*, Sep. 2015, pp. 96–101.

[41] T. R. Oliveira, F. J. A. Andrade, A. M. Picorone, H. A. Latchman, S. L. Netto, and M. V. Ribeiro, "Characterization of hybrid communication channel in indoor scenario," *J. of Communication and information Systems*, vol. 31, no. 1, pp. 224–235, Dec. 2016.

[42] P. Kiedrowski, B. Boryna, and T. Marciniak, "Last-mile smart grid communications based on hybrid technology as a reliable method of data acquisition and distribution," *Rynek Energii*, pp. 127–132, Feb. 2013.

[43] S. W. Lai and G. G. Messier, "Using the wireless and PLC channels for diversity," *IEEE Trans. Commun.*, vol. 60, no. 12, pp. 3865–3875, Dec. 2012.

[44] M. Sayed and N. Al-Dhahir, "Narrowband-PLC/wireless diversity for smart grid communications," in *Proc. IEEE Global Commun. Conf.*, Dec. 2014, pp. 2966–2971.

[45] S. W. Lai and G. G. Messier, "The wireless/power-line diversity channel," in *Proc. IEEE Int. Conf. on Commun.*, May. 2010, pp. 1–5.

[46] V. Fernandes, M. L. Filomeno, W. A. Finamore, and M. V. Ribeiro, "An investigation on narrow band PLC-wireless parallel channel capacity," in *Proc. XXXIV Simpósio Brasileiro de Telecomunicações*, Sep. 2016, pp. 834–838.

[47] J. Medbo and P. Schramm, "Channel models for hiperlan/2 in different indoor scenarios," ETSI EP, BRAN Meeting # 3, Technical Report 3ERI085B.

[48] A. J. Goldsmith and M. Effros, "The capacity region of broadcast channels with intersymbol interference and colored gaussian noise," *IEEE Trans. Inf. Theory*, vol. 47, no. 1, pp. 219–240, Jan. 2001.

[49] C. Choudhuri and U. Mitra, "Capacity bounds for relay channels with intersymbol interference and colored gaussian noise," *IEEE Trans. Inf. Theory*, vol. 60, no. 9, pp. 5639–5652, Sep. 2014.

[50] J. Long, M. Dong, K. Ota, and A. Liu, "A green tdma scheduling algorithm for prolonging lifetime in wireless sensor networks," *IEEE Systems Journal*, vol. 11, no. 2, pp. 868–877, June 2017.

[51] M. Dong, K. Ota, A. Liu, and M. Guo, "Joint optimization of lifetime and transport delay under reliability constraint wireless sensor networks," *IEEE Transactions on Parallel and Distributed Systems*, vol. 27, no. 1, pp. 225–236, Jan. 2016.

[52] T. M. Cover and J. A. Thomas, *Elements of Information Theory*. Wiley-Interscience, 2006.

[53] L. R. Ford and D. R. Fulkerson, *Flows in Networks*. Princeton University Press, 1962.

[54] T. R. Oliveira, C. A. G. Marques, W. A. Finamore, S. L. Netto, and M. V. Ribeiro, "A methodology for estimating frequency responses of electric power grids," *Journal of Control, Automation and Electrical Systems*, vol. 25, no. 6, pp. 720–731, Sep. 2014.

[55] M. Patzold, *Mobile Radio Channels*, 2nd ed. John Wiley & Sons, Ltd, 2011.

[56] J. Khun-Jush, P. Schramm, G. Malmgren, and J. Torsner, "Hiperlan2: broadband wireless communications at 5 ghz," *IEEE Communications Magazine*, vol. 40, no. 6, pp. 130–136, Jun 2002.

[57] T. R. Oliveira, A. A. M. Picorone, S. L. Netto, and M. V. Ribeiro, "Characterization of brazilian in-home power line channels for data communication," *Electric Power Systems Research*, vol. 150, pp. 188–197, 2017.

APPENDIX A – AF and DF achievable data rates

Based on the AF protocol, one can come up with a SRC model, which is constituted by $\mathcal{S}$, $\mathcal{R}$, and $\mathcal{D}$ nodes. According to [20], the received symbol at $\mathcal{D}$ node can be written as

$$\begin{aligned}\mathbf{Y}_{\mathcal{D}}^{'} &= \begin{bmatrix}\mathbf{Y}_{\mathcal{D},1}\\ \mathbf{Y}_{\mathcal{D},2}\end{bmatrix}\\ &= \begin{bmatrix}\mathbf{\Lambda}_{\sqrt{P_{\mathcal{S}}}}\mathbf{\Lambda}_{\mathbf{H}_{\mathcal{SD}}}\mathbf{X}+\mathbf{V}_{\mathcal{SD}}\\ \mathbf{\Lambda}_{\sqrt{P_{\mathcal{R}}}}\mathbf{\Lambda}_{P_{\mathbf{Y}_{\mathcal{R}}}}^{-1/2}\mathbf{\Lambda}_{\mathbf{H}_{\mathcal{RD}}}(\mathbf{\Lambda}_{\sqrt{P_{\mathcal{S}}}}\mathbf{\Lambda}_{\mathbf{H}_{\mathcal{SR}}}\mathbf{X}+\mathbf{V}_{\mathcal{SR}})+\mathbf{V}_{\mathcal{D}}\end{bmatrix},\end{aligned} \tag{A.1}$$

in which $\mathbf{Y}_{\mathcal{D},1}$ and $\mathbf{Y}_{\mathcal{D},2}$ denote the received symbols in the first and second time slots, respectively, and $\mathbf{\Lambda}_{P_{\mathbf{Y}_{\mathcal{R}}}} = \mathbf{\Lambda}_{P_{\mathcal{S}}}\mathbf{\Lambda}_{|\mathbf{H}_{\mathcal{SR}}|^2} + \mathbf{\Lambda}_{P_{\mathbf{V}_{\mathcal{SR}}}}$ is the power of the received symbol at $\mathcal{R}$ node. The combination of these vectors results in

$$\mathbf{Y}_{\mathcal{D}} = \begin{bmatrix}\mathbf{D}_1 & \mathbf{D}_2\end{bmatrix}\mathbf{Y}_{\mathcal{D}}^{'}, \tag{A.2}$$

in which matrices $\mathbf{D}_1$ and $\mathbf{D}_2$ are presented in Table 1 for MRC. Note that $\mathbf{Y}_{\mathcal{D}}$ can be rewritten as follows:

$$\mathbf{Y}_{\mathcal{D}} = \mathbf{A}_1\mathbf{X} + \mathbf{B}_1\mathbf{V}_1, \tag{A.3}$$

where $\mathbf{V}_1 = [\mathbf{V}_{\mathcal{SD}}^T\mathbf{V}_{\mathcal{SR}}^T\mathbf{V}_{\mathcal{RD}}^T]^T$,

$$\mathbf{A}_1 = \mathbf{D}_1\mathbf{\Lambda}_{\sqrt{P_{\mathcal{S}}}}\mathbf{\Lambda}_{\mathbf{H}_{\mathcal{SD}}} + \mathbf{D}_2\mathbf{\Lambda}_{\sqrt{P_{\mathcal{S}}}}\mathbf{\Lambda}_{\sqrt{P_{\mathcal{R}}}}\mathbf{\Lambda}_{P_{\mathbf{Y}_{\mathcal{R}}}}^{-1/2}\mathbf{\Lambda}_{\mathbf{H}_{\mathcal{SR}}}\mathbf{\Lambda}_{\mathbf{H}_{\mathcal{RD}}}, \tag{A.4}$$

and

$$\mathbf{B}_1 = [\mathbf{D}_1 \quad \mathbf{D}_2\mathbf{\Lambda}_{\sqrt{P_{\mathcal{R}}}}\mathbf{\Lambda}_{P_{\mathbf{Y}_{\mathcal{R}}}}^{-1/2}\mathbf{\Lambda}_{\mathbf{H}_{\mathcal{RD}}} \quad \mathbf{D}_2]. \tag{A.5}$$

Therefore,

$$f_{AF}(\mathcal{I}_{\mathcal{SD}}, \mathcal{I}_{\mathcal{SR}}, \mathcal{I}_{\mathcal{RD}}) = \max_{\mathbf{\Lambda}_{P_i}} \frac{B_w}{N\,N_T}\log_2[\det(\mathbf{I}_N + \mathbf{E}_1/\mathbf{F}_1)], \tag{A.6}$$

subject to $\sum\limits_i \mathrm{Tr}(\mathbf{\Lambda}_{P_i}) \leq P$, with $i \in \{\mathcal{S}, \mathcal{R}\}$ and $N_T = 2$, where $\mathbf{E}_1 = \mathbf{A}_1\mathbf{R}_{\mathbf{XX}}\mathbf{A}_1^{\dagger}$ and $\mathbf{F}_1 = \mathbf{B}_1\mathbf{R}_{\mathbf{V}_1\mathbf{V}_1}\mathbf{B}_1^{\dagger}$. Also, remind that $\mathcal{I}_{ij}$ represents $\mathbf{\Lambda}_{P_i}$, $\mathbf{\Lambda}_{|\mathbf{H}_{ij}|^2}$ and $\mathbf{\Lambda}_{P_{\mathbf{V}_{ij}}}$.

Table 1: Decision matrices for MRC in the first and second time slots.

$\mathbf{D}_1$	$\frac{\mathbf{\Lambda}_{\mathbf{H}_{\mathcal{SD}}}^{\dagger}}{\mathbf{\Lambda}_{P_{\mathbf{V}_{\mathcal{SD}}}}}$
$\mathbf{D}_2$	$\frac{\mathbf{\Lambda}_{\sqrt{P_{\mathcal{R}}}}\mathbf{\Lambda}_{P_{\mathbf{Y}_{\mathcal{R}}}}^{-1/2}\mathbf{\Lambda}_{\mathbf{H}_{\mathcal{SR}}}^{\dagger}\mathbf{\Lambda}_{\mathbf{H}_{\mathcal{RD}}}^{\dagger}}{\mathbf{\Lambda}_{P_{\mathcal{R}}}\mathbf{\Lambda}_{P_{\mathbf{Y}_{\mathcal{R}}}}^{-1}\mathbf{\Lambda}_{\lvert\mathbf{H}_{\mathcal{RD}}\rvert^2}\mathbf{\Lambda}_{P_{\mathbf{V}_{\mathcal{SR}}}}+\mathbf{\Lambda}_{P_{\mathbf{V}_{\mathcal{RD}}}}}$

Regarding the DF protocol, according to [49] and assuming that the relay is error-free, it possible to write

$$f_{DF}(\mathcal{I}_{\mathcal{SD}}, \mathcal{I}_{\mathcal{SR}}, \mathcal{I}_{\mathcal{RD}}) = \min\{C_{DF,1}, C_{DF,2}\}, \tag{A.7}$$

in which $C_{DF,1} = 0.5\ C_{\mathcal{SR}}$ and

$$C_{DF,2} = \max_{\mathbf{\Lambda}_{P_i}} \frac{B_w}{N\,N_T} \log_2[\det(\mathbf{I}_N + \mathbf{\Lambda}_{\gamma_{\mathcal{SD}}} + \mathbf{\Lambda}_{\gamma_{\mathcal{RD}}})], \tag{A.8}$$

subject to $\sum\limits_i \mathrm{Tr}(\mathbf{\Lambda}_{P_i}) \leq P$, with $i \in \{\mathcal{S}, \mathcal{R}\}$ and $N_T = 2$.

APPENDIX B – SNR for configuration E

Initially, assume that $\mathbf{Y}_{R_b}$ is the received symbol at R_b node given by (A.3), but regarding $\mathcal{S} = S$, $\mathcal{R} = R_a$, and $\mathcal{D} = R_b$. Also, consider that the transmitted symbol by R_b node, $\mathbf{X}_{R_b}$, is given by

$$\mathbf{X}_{R_b} = \mathbf{\Lambda}_{P_{\mathbf{Y}_{R_b}}}^{-1/2} \mathbf{Y}_{R_b}, \tag{B.1}$$

where $\mathbf{\Lambda}_{P_{\mathbf{Y}_{R_b}}} = \mathbb{E}\{\mathbf{Y}_{R_b}\mathbf{Y}_{R_b}^{\dagger}\}/N = (\mathbf{E}_1+\mathbf{F}_1)/N$. Thus, using the same structure of (A.1) to represent the received symbol at D node, $\mathbf{Y}_D^{'}$, but with $\mathbf{X}_{R_b}$ instead of $\mathbf{X}$ and considering $\mathbf{\Lambda}_{P_{\mathbf{Y}_{R_c}}} = \mathbf{\Lambda}_{|\mathbf{H}_{R_bR_c}|^2}\mathbf{\Lambda}_{P_{R_b}} + \mathbf{\Lambda}_{P_{\mathbf{V}_{R_bR_c}}}$, as in (B.5). Applying MRC, one have

$$\mathbf{Y}_D = \begin{bmatrix}\mathbf{D}_3 & \mathbf{D}_4\end{bmatrix} \mathbf{Y}_D^{'}, \tag{B.2}$$

in which matrices $\mathbf{D}_3$ and $\mathbf{D}_4$ are detailed in Table 2 for MRC. Now, given matrices $\mathbf{A}_2$ and $\mathbf{B}_2$, which are described by (B.6) and (B.7), the following equations arise:

$$\mathbf{Y}_D = \mathbf{A}_2\mathbf{X} + \mathbf{B}_2\mathbf{V}_2, \tag{B.3}$$

in which $\mathbf{V}_2 = [\mathbf{V}_1^T\mathbf{V}_{R_bD}^T\mathbf{V}_{R_bR_c}^T\mathbf{V}_{R_cD}^T]^T$. As a result, the SNR matrix for the configuration E is given by

$$\mathbf{\Lambda}_{\gamma_{E,AF}} = \mathbf{A}_2\mathbf{R}_{\mathbf{XX}}\mathbf{A}_2^{\dagger}(\mathbf{B}_2\mathbf{R}_{\mathbf{V}_2\mathbf{V}_2}\mathbf{B}_2^{\dagger})^{-1}. \tag{B.4}$$

$$
\begin{aligned}
\mathbf{Y}_D^{'} &= \begin{bmatrix} \mathbf{Y}_{D,3} \\ \mathbf{Y}_{D,4} \end{bmatrix} \\
&= \begin{bmatrix} \mathbf{\Lambda}_{\sqrt{P_{R_b}}} \mathbf{\Lambda}_{\mathbf{H}_{R_b D}} \mathbf{X}_{R_b} + \mathbf{V}_{R_b D} \\ \mathbf{\Lambda}_{\sqrt{P_{R_c}}} \mathbf{\Lambda}_{P_{\mathbf{Y}_{R_c}}}^{-1/2} \mathbf{\Lambda}_{\mathbf{H}_{R_c D}} \left(\mathbf{\Lambda}_{\sqrt{P_{R_b}}} \mathbf{\Lambda}_{\mathbf{H}_{R_b R_c}} \mathbf{X}_{R_b} + \mathbf{V}_{R_b R_c} \right) + \mathbf{V}_{R_c D} \end{bmatrix} \\
&= \begin{bmatrix} \mathbf{\Lambda}_{\sqrt{P_{R_b}}} \mathbf{\Lambda}_{P_{\mathbf{Y}_{R_b}}}^{-1/2} \mathbf{\Lambda}_{\mathbf{H}_{R_b D}} \left(\mathbf{A}_1 \mathbf{X} + \mathbf{B}_1 \mathbf{V}_1 \right) + \mathbf{V}_{R_b D} \\ \mathbf{\Lambda}_{\sqrt{P_{R_b}}} \mathbf{\Lambda}_{\sqrt{P_{R_c}}} \mathbf{\Lambda}_{P_{\mathbf{Y}_{R_b}}}^{-1/2} \mathbf{\Lambda}_{P_{\mathbf{Y}_{R_c}}}^{-1/2} \mathbf{\Lambda}_{\mathbf{H}_{R_c D}} \mathbf{\Lambda}_{\mathbf{H}_{R_b R_c}} \left(\mathbf{A}_1 \mathbf{X} + \mathbf{B}_1 \mathbf{V}_1 \right) + \mathbf{\Lambda}_{\sqrt{P_{R_c}}} \mathbf{\Lambda}_{P_{\mathbf{Y}_{R_c}}}^{-1/2} \mathbf{\Lambda}_{\mathbf{H}_{R_c D}} \mathbf{V}_{R_b R_c} + \mathbf{V}_{R_c D} \end{bmatrix}
\end{aligned} \tag{B.5}
$$

$$
\mathbf{A}_2 = \left(\mathbf{D}_3 \mathbf{\Lambda}_{\mathbf{H}_{R_b D}} + \mathbf{D}_4 \mathbf{\Lambda}_{\sqrt{P_{R_c}}} \mathbf{\Lambda}_{P_{\mathbf{Y}_{R_c}}}^{-1/2} \mathbf{\Lambda}_{\mathbf{H}_{R_c D}} \mathbf{\Lambda}_{\mathbf{H}_{R_b R_c}} \right) \mathbf{\Lambda}_{\sqrt{P_{R_b}}} \mathbf{\Lambda}_{P_{\mathbf{Y}_{R_b}}}^{-1/2} \mathbf{A}_1 \tag{B.6}
$$

$$
\mathbf{B}_2 = [(\mathbf{D}_3 \mathbf{\Lambda}_{\mathbf{H}_{R_b D}} + \mathbf{D}_4 \mathbf{\Lambda}_{\sqrt{P_{R_c}}} \mathbf{\Lambda}_{P_{\mathbf{Y}_{R_c}}}^{-1/2} \mathbf{\Lambda}_{\mathbf{H}_{R_c D}} \mathbf{\Lambda}_{\mathbf{H}_{R_b R_c}}) \mathbf{\Lambda}_{\sqrt{P_{R_b}}} \mathbf{\Lambda}_{P_{\mathbf{Y}_{R_b}}}^{-1/2} \mathbf{B}_1 \quad \mathbf{D}_3 \quad \mathbf{D}_4 \mathbf{\Lambda}_{\sqrt{P_{R_c}}} \mathbf{\Lambda}_{P_{\mathbf{Y}_{R_c}}}^{-1/2} \mathbf{\Lambda}_{\mathbf{H}_{R_c D}} \quad \mathbf{D}_4] \tag{B.7}
$$

Table 2: Decision matrices for MRC in the third and fourth time slots.

$\mathbf{D}_3$	$\frac{\mathbf{\Lambda}_{\mathbf{H}_{R_b D}}^{\dagger}}{\mathbf{\Lambda}_{P_{R_b}} \mathbf{\Lambda}_{P_{\mathbf{Y}_{R_b}}}^{-1} \mathbf{\Lambda}_{\lvert \mathbf{H}_{R_b D} \rvert^2 \mathbf{F}_1 + \mathbf{\Lambda}_{P_{\mathbf{V}_{R_b D}}}}}$
$\mathbf{D}_4$	$\frac{\mathbf{\Lambda}_{\sqrt{P_{R_c}}} \mathbf{\Lambda}_{P_{\mathbf{Y}_{R_c}}}^{-1/2} \mathbf{\Lambda}_{\mathbf{H}_{R_b R_c}}^{\dagger} \mathbf{\Lambda}_{\mathbf{H}_{R_c D}}^{\dagger}}{\mathbf{\Lambda}_{P_{R_c}} \mathbf{\Lambda}_{P_{\mathbf{Y}_{R_c}}}^{-1} \mathbf{\Lambda}_{\lvert \mathbf{H}_{R_c D} \rvert^2} (\mathbf{\Lambda}_{P_{R_b}} \mathbf{\Lambda}_{P_{\mathbf{Y}_{R_b}}}^{-1} \mathbf{\Lambda}_{\lvert \mathbf{H}_{R_b R_c} \rvert^2 \mathbf{F}_1 + \mathbf{\Lambda}_{P_{\mathbf{V}_{R_b R_c}}}}) + \mathbf{\Lambda}_{P_{\mathbf{V}_{R_c D}}}}$

APPENDIX C – Specification of the 18-path HIPERLAN/2 for typical office environments.

Table 3: Specification of the 18-path HIPERLAN/2 for typical office environments [47].

Path Number	Propagation Delay (ns)	Relative Path Power [linear]	Relative Path Power [dB]	Rice Factor	Doppler PSD	Delay spread (ns)
1	0	1.0000	0.0	0	"Jakes"	50
2	10	0.1259	−0.9			
3	20	0.6761	−1.7			
4	30	0.5495	−3.5			
6	50	0.3715	−4.3			
7	60	0.3020	−5.2			
8	70	0.2455	−6.1			
9	80	0.2042	−6.9			
10	90	0.1660	−7.8			
11	110	0.3388	−4.7			
12	140	0.1862	−7.3			
13	170	0.1023	−9.9			
14	200	0.0562	−12.5			
15	240	0.0427	−13.7			
16	290	0.0159	−18.0			
17	340	0.0058	−22.4			
18	390	0.0021	−26.7			

APPENDIX D – PLC Channel Frequency Responses

In order to give an idea about the behavior of the PLC CFRs used throughout this work, Fig. 12 shows the CFR average magnitudes of the PLC channel estimates obtained from the measurement campaign for all analyzed cases.

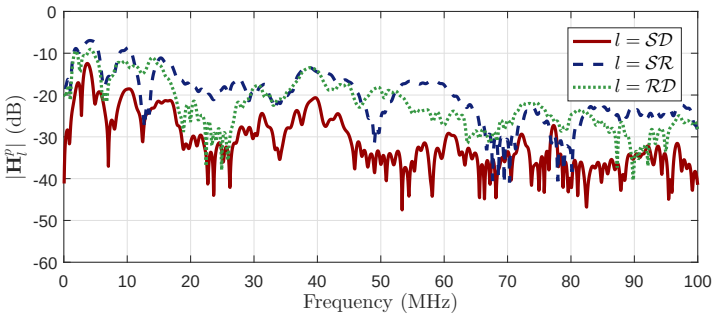

(a)

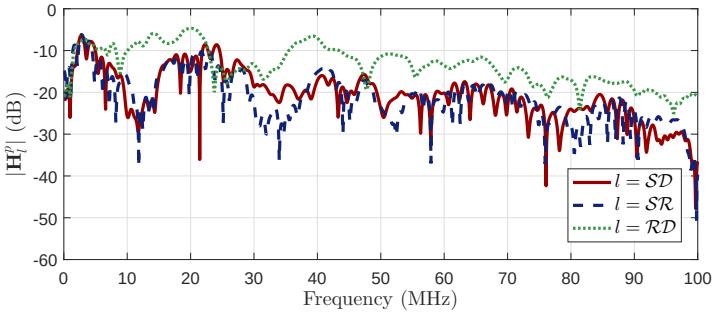

(b)

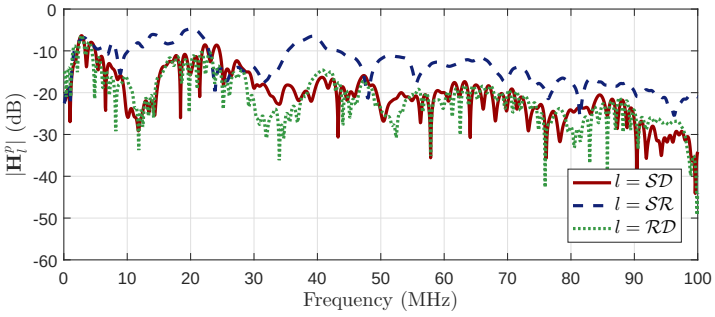

(c)

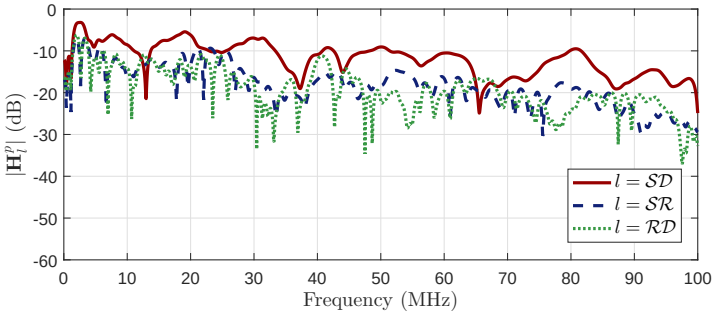

(d)

Figure 12: Magnitude of average PLC CFRs. (a) case #1, (b) case #2, (c) case #3, and (d) case #4.

APPENDIX E – Wireless Channel Frequency Responses

With the same aim of the Appendix D, Fig. 13 shows the CFR average magnitudes of the wireless channel estimates obtained from the HIPERLAN/2 standard for all analyzed cases.

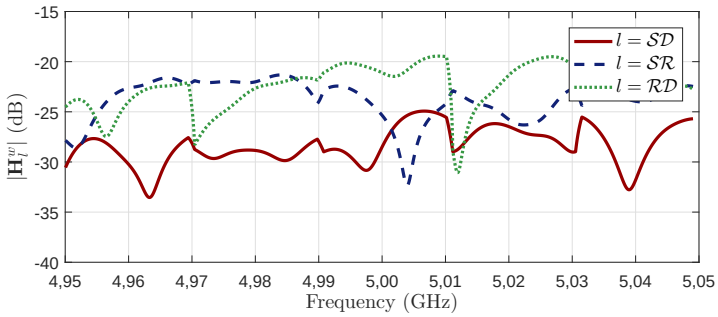

(a)

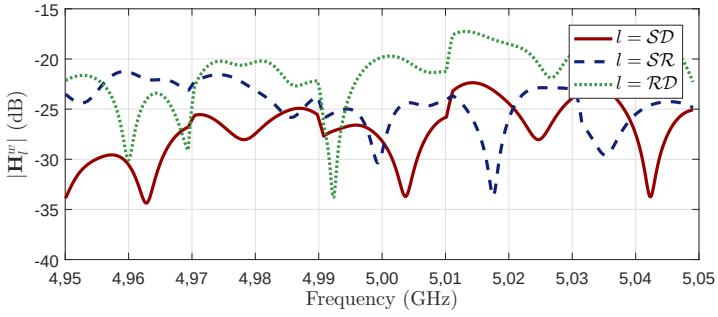

(b)

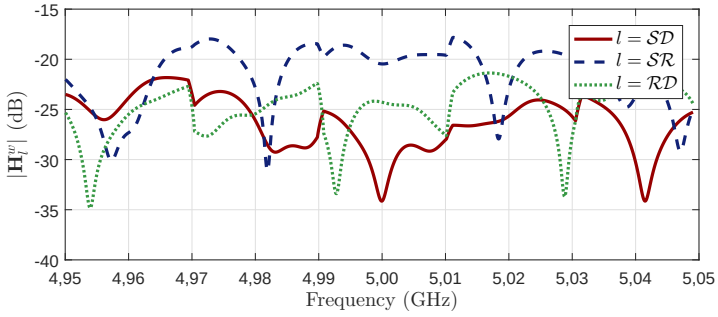

(c)

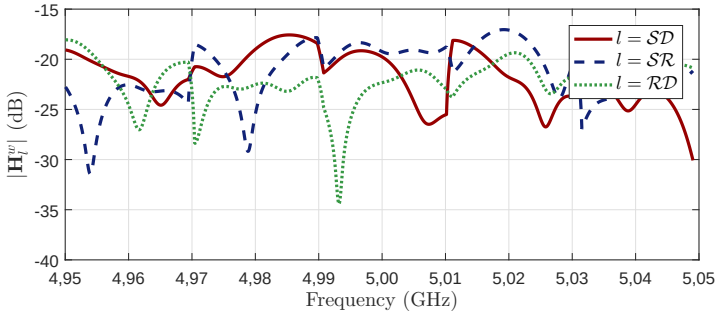

(d)

Figure 13: Magnitude of average wireless CFRs. (a) case #1, (b) case #2, (c) case #3, and (d) case #4.

APPENDIX F – List of Publications

The list of conference papers published during the graduate period is as follows:

- M. de L. Filomeno, V. Fernandes, and M. V. Ribeiro, "Análise estatística da capacidade de canais PLC residenciais cooperativos baseada no modelo single relay channel," in *Proc. XXXIV Simpósio Brasileiro de Telecomunicações*, Sep. 2016, pp. 843-847.

- V. Fernandes, M. de L. Filomeno, W. A. Finamore, and M. V. Ribeiro, "An investigation on narrow band PLC-wireless parallel channel capacity," in *Proc. XXXIV Simpósio Brasileiro de Telecomunicações*, Sep. 2016, pp. 834-838.

The journal paper published during the graduate period is as follows:

- L. de M. B. A. Dib, V. Fernandes, M. de L. Filomeno, and M. V. Ribeiro, "Hybrid PLC/Wireless Communication For Smart Grids and Internet of Things Applications," *IEEE Internet of Things Journal*, vol. PP, no. 99, pp. 1-13, 2017.